A Calibration Method for a Controlled Reception Pattern Antenna and Software Defined Radio Configuration

A thesis presented to

the faculty of

the Russ College of Engineering and Technology of Ohio University

In partial fulfillment

of the requirements for the degree

Master of Science

Zachary Obenour Bauer

May 2013

This thesis titled

A Calibration Method for a Controlled Reception Pattern Antenna and Software Defined Radio Configuration

by

ZACHARY OBENOUR BAUER

has been approved for

the School of Electrical Engineering and Computer Science

and the Russ College of Engineering and Technology by

Chris G. Bartone

Professor of Electrical Engineering and Computer Science

Dennis Irwin

Dean, Russ College of Engineering and Technology

ABSTRACT

BAUER, ZACHARY OBENOUR., M.S., May 2013, Electrical Engineering

A Calibration Method for a Controlled Reception Pattern Antenna and Software Defined Radio Configuration

Director of Thesis: Chris G. Bartone

This thesis presents a demonstrated method for the performance of a calibration method for a controlled reception pattern antenna (CRPA) using a Software Defined Radio (SDR) configuration. The combination CRPA and SDR system consists of a low-cost 7-element configuration where the antenna RF inputs are feed directly into the multi-channel SDR system. This combination CRPA and SDR system was characterized in an anechoic chamber environment to closely replicate the fielded antenna/receiver system. This combined CRPA and SDR system calibration method configuration can provide multi-antenna element characterization and calibration measurements that can be used to remove carrier and code phase biases caused by the antenna elements and receiver front-end components for down-stream adaptive signal processing algorithms. For verification, the calibration data produced by the CRPA/SDR system configuration will be compared with calibration data produced using a traditional CRPA anechoic chamber test approach where each element of the array is characterized one at a time with a traditional antenna test approach.

ACKNOWLEDGMENTS

First and foremost, I would like to thank my advisor, Dr. Chris Bartone, for his support and guidance throughout my thesis. He gave me direction and invaluable assistance which enabled me to complete my research. I would also like to thank Dr. Sanjeev Gunawardena for allowing me to use the TRIGR software defined radio data collection system he developed. He provided patient encouragement and expert advice and was always more than willing to answer any questions that I had. I would also like to thank Dr. Michael Braasch and Dr. David Ingram for their help and counsel. I am very grateful for their assistance. Finally, I would like to thank my parents for their endless support and encouragement. They have instilled in me a strong work ethic and curiosity to learn and without them I would not have achieved my goals.

TABLE OF CONTENTS

Page

LIST OF FIGURES

Page

LIST OF ACRONYMS

ADC	Analog-to-digital Converter
AGC	Automatic Gain Control
ARP	Aperture Reference Point
AUT	Antenna-under-test
Bn	Loop Filter Bandwidth
BPF	Band-pass Filter
CRPA	Controlled Reception Pattern Antenna
CSC	Carrier Smoothed Code
CW	Carrier Wave
DVGA	Digitally Controlled Variable Gain Amplifiers
FLL	Frequency Locked Loop
FPGA	Field-Programmable Gate Array
FRPA	Fixed Reception Pattern Antenna
GNSS	Global Navigation Satellite System
GPS	Global Positioning System
I	In-phase
IF	Intermediate Frequency
INS	Inertial Navigation System
LNA	Low-noise Amplifier
LO	Local Oscillator
LPF	Low-pass Filter

LVDS	Low-Voltage Differential Signaling
NCO	Numerically Controlled Oscillator
NGS	National Geodetic Survey
PDI	Pre-Detection Integration
PLL	Phased Locked Loop
PLO	Phased-Locked Oscillator
Q	Quadrature-phase
RF	Radio Frequency
RF-BPF	Radio Frequency Band-pass Filter
RHCP	Right Hand Circularly Polarized
SDR	Software Defined Radio
SMA	SubMiniature version A
STAP	Space-Time Adaptive Processing
SV	Satellite Vehicle
TOA	Time-of-arrival
TRIGR	Transform-Domain Instrumentation GNSS Receiver
VNA	Vector Network Analyzer

CHAPTER 1 INTRODUCTION

Spread-spectrum ranging systems, such as the Global Positioning System (GPS), provide position and timing estimations for a large variety of consumer and military applications. To maintain system performance in any operational environment, the user GPS receiver/antenna must operate in the presence of signal interference (intentional or unintentional) and noise. Error mitigation techniques can be implemented within the antenna and receiver design architecture to reduce the effects of signal interference and provide high-accuracy position solutions.

GPS is a satellite-based passive ranging system that enables three-dimensional user position solutions. This is achieved through a process known as trilateration. Using trilateration, a GPS receiver determines the time-of-arrival (TOA) of time-synchronized radio frequency (RF) signals transmitted from orbiting satellite vehicles (SVs) within the receiver's field-of-view. Each SV transmits a GPS signal that includes an RF carrier signal, ranging code, and navigation data. The receiver uses this information to estimate the distance between the user and the SVs in terms of transit time; these range measurements are known as pseudoranges. The pseudorange measurements allow the receiver to estimate user position and clock bias; in order for the receiver to accurately estimate the user's position, a minimum of four SVs must be in view [1].

GPS is often used for navigation and timing systems. In the past twenty years, the use of GPS for accurate position and timing system applications has grown significantly [2] [3] [4]. In navigation systems, GPS is used to aid flight path determination and precision approach and landing systems [4] [5] [6] [7]. Precision landing applications rely on highly accurate code and carrier phase measurements and should operate in the presence of multiple interference sources such as multipath, noise and jammers. With such vital applications dependent on GPS, it is important that unwanted interference does not hinder its performance and introduce errors that could render the system useless [8].

One of the largest sources of interference is multipath [9]. Multipath can contribute to large code and carrier phase measurement errors in the GPS receiver system. Multipath occurs when transmitted signals are reflected off the ground or by nearby objects, thereby delaying the arrival of the multipath signal. These undesired delayed multipath signals combine with the direct signal and can interfere with the tracking loops and correlation algorithms implemented by the receiver to maintain synchronization with the desired/direct incoming signal. The synchronization accuracy of the receiver's tracking loop determines the accuracy of the carrier and code phase measurements and eventually the user's position and time estimate [9].

Jammers and other high power transmission emitters can also induce interference in a GPS receiver system. GPS reception antennas operate on signals at very low power levels, well below the thermal noise floor (-157 dBW) [8]. Because of this, any nearby transmission system operating above the noise floor in the GPS frequency band can induce unwanted interference and measurement errors in the receiver system.

To reduce signal interference and improve the overall performance of the receiver systems, various error mitigation techniques can be employed. The fundamental necessity for any error mitigation technique is to help maintain the signal-to-interference plus noise ratio (SINR). This is done by removing unwanted noise and interference in the receiver system, while maintaining a lock on the desired satellite signal. Signal interference and measurement bias on the received signal can be reduced through a variety of error mitigation techniques such as, antenna design, integrated multi-sensor systems, advanced signal processing, or by implementing beam forming and/or null steering algorithms using a multi-element phased antenna array.

Through antenna design, various antenna radiation beam patterns can be produced. With a fixed reception pattern antenna (FRPA), the main beam of the antenna pattern remains fixed but can be directed toward the desired signals to reduce unwanted interference through side lobe suppression. Often ground-based reception antennas will be designed to reduce the gain in the lower hemisphere of the radiation pattern, where the effects of multipath interference are most predominant [3]. These methods are typically easier to implement, but may become less effective in the presence of jammers; especially as the jamming interference source approaches the location of the desired signal [4]. Unwanted interference and multipath can come from any direction in the receiver's antenna pattern leaving a receiver that uses a FRPA susceptible to phase and measurement errors [10].

Multi-sensor measurement systems, such as a GPS receiver integrated with an inertial navigation system (INS), are utilized in navigation systems to compensate for measurement errors produced by each individual system. An INS relies on integrated accelerometer and gyroscope measurements to determine the change in three-dimensional displacement and rotation of the moving vehicle. INS are susceptible to gryo drift and accelerometer errors, resulting in an accumulated measurement biases over time;

whereas, GPS receiver systems are vulnerable to more random measurement noise that is largely unbiased in the long term. To limit the measurement errors produced by each system, the INS can provide external aiding to the GPS receiver tracking loop and GPS measurements can be used to minimize the INS drift errors. Typically the GPS and INS measurements are combined in a Kalman Filter. A properly tuned Kalman Filter can produce low noise, low bias position, velocity, and time estimates. Multi-sensor measurement systems, relying on satellite based position sensors, are still susceptible to signal interference such as multipath and jammers [11].

Beam forming and/or null steering techniques can be implemented to reduce signal intference using a multi-element phased antenna array. With a phased antenna array system, the phase response and spacing between each individual antenna element is assumed to be known. When an incoming signal is received by the phased antenna array it will excite one antenna element first then, shortly after, excite the other antenna elements of the system. The time delay and corresponding phase shift, that each antenna element senses, can be correlated and used to determine the direction of the received signal [10]. This information can be used to implement signal processing and spatial processing techniques to further mitigate erroneous and biased data in the reception system [12], allowing for an improved user solution.

A Controlled Reception Pattern Antenna (CRPA) can implement beam forming and/or null steering techniques to improve the overall performance of the antenna, especially in the presence of multiple interfering signals such as jammers [13]. By implementing beam forming and/or null steering techniques, CRPAs can provide anti-jamming capabilities to avoid unwanted interference. Anti-jamming is achieved by steering the main beam of the CRPA antenna pattern toward the desired signal and/or placing nulls at the geometric location of unwanted interference sources in the antenna pattern [7].

A CRPA receiver system's antenna hardware, front-end electronics, and adaptive processing algorithms introduce measurement biases to the system [5] [6] [7] [14] [15], which can result in significant measurement error. The receiver system's antenna elements are susceptible to phase variations, dependent on the elevation angle of the incoming satellite signal [16], as well as the antenna elements placement within the array. This can lead to inaccurate phase estimations needed by the receiver to resolve a user solution. Thermal noise amplification within the analog components of the receiver system's front-end electronics can introduce further measurement biases to the system. Multi-antenna element array systems induce additional measurement biases as a result of mutual coupling between elements and fringing effects on the edges of the CRPAs ground plane [5] [6]. To reduce measurement biases produced by the CRPA hardware and front-end components, the receiver system most often will need to be calibrated depending on the user solution requirements.

Calibration procedures are performed for many GNSS antennas for various applications [17]. For high accuracy applications (e.g., geodetic), an antenna look-up table of calibration parameters [18], consisting of phase delays and amplitude adjustment, can be applied to the signal measurements to correct for measurement biases within the antenna. The calibration parameters are determined by testing the individual antenna element and measuring the phase and amplitude variations introduced by the antenna hardware [16]. Calibration testing can be performed in an anechoic chamber [19] [20] where no signal interference is present or by testing with the outdoor GPS signals using a reference element and implement differential signal processing techniques to remove common-mode errors between the two antennas [16].

Additional consideration must be taken into account regarding the calibration requirements for a CRPA receiver system implementing beam forming and null steering techniques. Each antenna element of the array can inherently produce code and carrier phase biasing within the received satellite signals. In order for a CRPA reception system to adequately provide a high-accuracy user solution, the induced phase biases must be removed. To correct for the induced biases on the received signals by the antenna array, each antenna element of the CRPA must be calibrated [10]. Adaptive signal processing algorithms can be used to mitigate the effects of antenna induced biases; however, adaptive algorithms cannot remove all biases produced by the antenna hardware without predetermined calibration data for the antennas in the array [6].

Typical calibration procedures for a CRPA system test each antenna element of the array individually. In an anechoic chamber, each element is tested by connecting the antenna element under test to the receiver and attaching a 50Ω load to each of the remaining antenna elements of the CRPA. The calibration parameters are then applied to each antenna element individually to remove the induced biases and provide accurate phase measurements. This calibration procedure accounts for the measurement biases induced by the hardware of each antenna element of the array. Adding the 50Ω loads to each element not under test acts like a perfect impedance match within the system. With an actual setup, there is additional impedance mismatch present within the system. To provide a more realized setup, each antenna element of the CRPA can be tested simultaneously using a multi-channel data acquisition system.

1.1 Scope

The focus of this thesis was to test and analyze in an anechoic chamber the performance of a CRPA using a multi-channel data acquisition receiving system. In real world applications each element of an antenna array receives signals simultaneously and continuously. However, typical range measurement testing can only capture data from one antenna element at a time. The goal of this research is to develop a data collection system that will capture signal responses from each antenna element simultaneously. This is possible through the use of a multi-channel data acquisition system. The antenna biases for the array can be determined from the measured data to obtain the calibration weights for the antenna-under-testing (AUT) [10]. By implementing a multi-channel data acquisition system, real world applications can be represented during range measurement testing.

This thesis presents a demonstrated method for the performance of a calibration method for a CRPA using a Software Defined Radio (SDR) configuration. The combination CRPA and SDR system consists of a low-cost 7-element configuration where the antenna RF inputs are feed directly into the multi-channel SDR system. This combination CRPA and SDR system was characterized in an anechoic chamber environment to closely replicate the fielded antenna/receiver system. This combined

CRPA and SDR system configuration will provide multi-antenna element characterization and calibration measurements that could be used to remove carrier and code phase biases caused by the antenna elements and receiver front-end components for down-stream adaptive signal processing algorithms. For verification, the calibration data produced by the CRPA/SDR system configuration was compared with calibration data produced using a traditional CRPA test approach where each element of the array is characterized one at a time with a traditional antenna test approach. While these test only characterized the carrier phase response of the AUT, it is believed that these test techniques can be expanded for both code and carrier phase characterization and calibration.

This thesis is organized as follows. Chapter 2 discusses the implementation and design of a CRPA array and provides an overview of beam forming and null steering fundamentals. Chapter 2 also discusses the processes of a digital receiver's front-end and the benefits of implementing a multi-channel measurement system using a combined CRPA/SDR receiver system. Chapter 3 details the induced measurement biases of a CRPA receiver system, provides an overview of antenna calibration procedures, discusses other CRPA calibration approaches, and presents the calibration method for a CRPA/SDR configuration demonstrated in this thesis. Chapter 4 examines the SDR front-end architecture utilized in the demonstrated calibration approach presented, and provides an overview of the baseband processing performed on the collected antenna data; detailing the various stages of the carrier tracking loop. Chapter 5 provides the CRPA/SDR configuration and method of testing used. This includes the antenna hardware specifications and CRPA design parameters, an overview of the anechoic chamber, and the calibration testing methods for both the traditional sequential single-channel measurement system and the CRPA/SDR multi-channel measurement system. Chapter 6 discusses the software baseband processing implemented during post processing, detailing the pre-detection integration time and loop filter parameters, the outlier correction, and cycle slip resolution methods used. Chapter 7 presents the testing results and provides data analysis. Chapter 8 includes conclusions and recommendations for future work.

CHAPTER 2 CONTROLLED RECEPTION PATTERN ANTENNA AND RECEVIER SYSTEMS

A controlled reception pattern antenna (CRPA) is a phased array that can be used to implement beam forming and/or null steering techniques to increase directivity towards a desired signal and mitigate unwanted interference, especially in the presence of multiple interference sources such as jammers [13]. The radiation pattern and antenna characteristics of a phased array are governed by the amplitude and phase of each individual antenna element, depends on the geometric configuration and location of each element in array [21], and the signal processing algorithm performed. CRPAs are advantageous for GPS reception because they can provide additional information about the direction of the incident received signal [10].

The receiver system estimates the pseudoranges and carrier phase measurements from the orbiting SVs by measuring the code and carrier phases of the received signals. Each transmitted SV signal is conditioned by the receiver's front-end before being processed by the baseband and receiver measurement processor. The receiver front-end amplifies, filters, down-converts, and samples the signals before digitally processing.

This chapter discusses design parameters for a CRPA array, and how beam forming/null steering techniques can be implemented to obtain the desired radiation pattern. The processes of a digital receiver's front-end will also be discussed, along with the benefits of implementing a multi-channel measurement system using a combined CRPA/SDR system.

2.1 CRPA Implementation and Design

A CRPA consists of individual antenna elements arranged in a particular pattern to enable increase directivity towards a desired signal and/or forming nulls in the direction of the interfering signal. Each antenna element of the CRPA is processed and combined to produce the desired radiation pattern. The size and amount of distortion present on the main beam is dependent on the number of antenna elements that comprise the CRPA [22]. Increasing the number of antenna elements used in the CRPA configuration will increase the degrees of freedom and allow for a more directive main beam that has a narrower beam width. Additionally, a CRPA comprised of N antenna elements is capable of mitigating $N-1$ interference sources. Therefore, increasing the number of antenna elements in a CRPA will allow more interference sources to be mitigated [22]. However, as the location of the interference source moves closer to the location of the desired signal, the main beam of the radiation pattern will become distorted, producing an asymmetrical shape [22].

The performance of the CRPA array is dependent on the location of each antenna element in the array [13]. A typical CRPA design used in GPS applications is a circular pattern, this allows the array to maintain two geometric degrees of freedom and direct the radiation pattern in multiple directions. When designing a circular CRPA array, the spacing and placement of each antenna element will affect the radiation pattern. Research shows [13] the best performance is achieved when each individual element is equally spaced along the perimeter in a circular configuration. In this configuration, each outer element is positioned around a center reference element. When the antenna elements are arranged in a circular pattern, the CRPA can receive signals from multiple directions, allowing for improved performance [10] [12]. This is due to the fact that GPS transmission and reception systems are right hand circularly polarized (RHCP).

The spacing of each outer element from the reference element and arc length from element to element is dependent on the frequency of the received signal and the receiver's application [8]. For optimal performance, each outer antenna element of the CRPA should be placed at a distance of $\lambda/2$ around the reference element [13]. Increasing the spacing between the outer elements and the reference element can introduce unwanted side lobes in the antenna's radiation pattern [23]. For a receiver operating within the GPS L1 band, the carrier wave signal is transmitted at 1575.42MHz and has a wavelength (λ) roughly equal to 19cm (7.48in). CRPAs operating within the GPS L1 frequency band typically space each outer element 3.74in ($\lambda/2$) from the reference element.

The AUT for this investigation was a constructed CRPA consisting of 7-active antenna elements, each mounted on a 14.12in circular ground plane. One reference element was placed in the center of the ground plane, with six outer elements mounted approximately 3.74in ($\lambda/2$) from the reference element. Figure 2-1 shows the CRPA configurations used in this investigation.

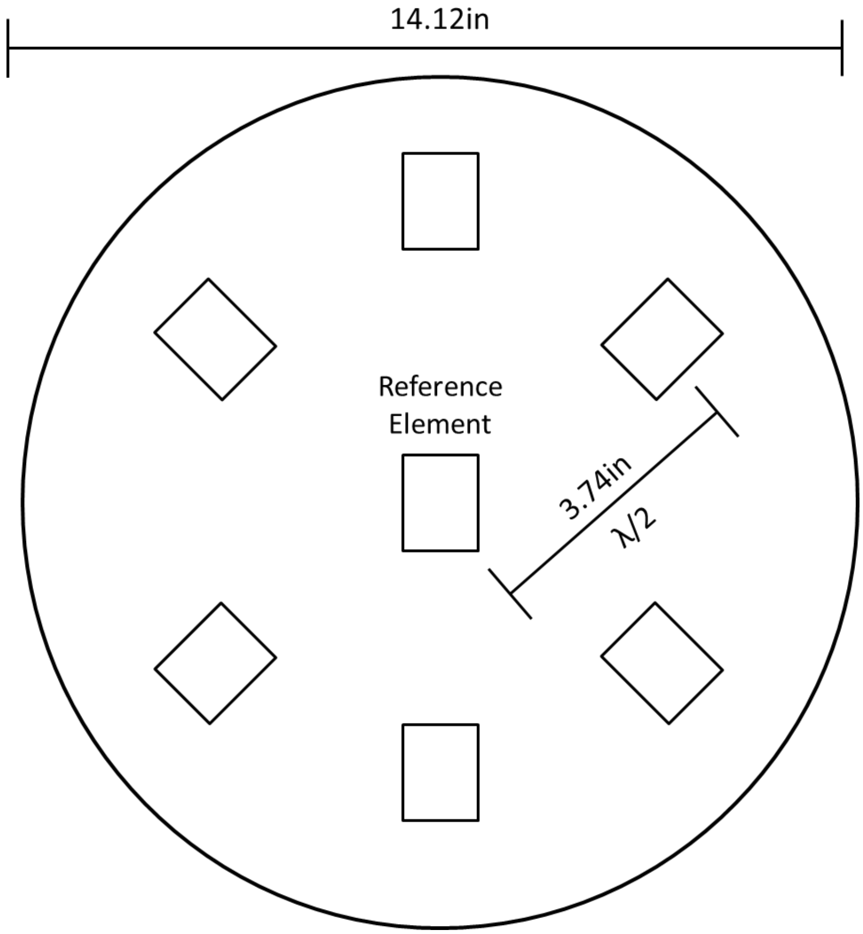

Figure 2-1. 7-Element CRPA circular configuration.

In a phased array antenna system, such as a CRPA, the spacing between each individual antenna element is known. When an incoming signal is received by the phased array, the signal will excite each antenna element at a different instant in time [24]. The time delay and phase shifts, that each antenna element senses, can be correlated and used to determine the direction of the incoming signal [10]. This information can be used to implement signal processing and spatial processing techniques [12] to further mitigate erroneous and biased data in the reception system, allowing for an improved position solution.

2.2 Beam Forming and/or Null Steering

With a CRPA array configuration, each antenna element is combined and processed to perform beam forming and/or null steering [8]. Implementing beam forming and null steering techniques allows the receiver to maintain maximum desired signal reception; this provides improved performance in the presence of multipath and unwanted interference [25] [12]. By implementing beam forming and null steering, CRPAs can produce anti-jamming capabilities to avoid intentional and unintentional interference. Anti-jamming is achieved by placing nulls in the antenna pattern at the location of interference sources [7].

Beam forming and null steering is performed by adjusting the amplitude and phase of the received signal for each antenna element in the array before combining. The amplitude and phase adjustments are known as complex weight. Applying complex weights to the output of each antenna element will steer the main lobe, side lobes, and nulls of the CRPAs antenna pattern. The complex weights vary from element to element depending on the reception pattern that is desired. Antenna pattern directionality is possible due to the electromagnetic interaction between each of the antenna elements [23].

Beam forming algorithms can be either deterministic or adaptive in nature. With a deterministic processing algorithm, the direction of the incoming signal must be known. The receiver applies the necessary phase and amplitude adjustment for each element to point the main lobe of the radiation pattern toward the known signal location. In order for the receiver to implement deterministic processing, the receiver must have prior knowledge of the necessary phase and amplitude adjustments needed to steer the beam in the desired direction. Adaptive beam forming adjusts the complex weights in real time to maintain the desired signal reception [8]. With adaptive beam forming processing, various weighting techniques can be applied [13] [26]. Weighting algorithms rely on certain criteria to govern the amount of complex weighting to apply and steer the beam and/or null in the desired direction. The criteria may be a maximum SINR threshold in which the receiver must maintain. If the signal reception falls below the threshold value, then the receiver will adaptively apply the necessary phase and amplitude adjustments to steer the beam until the criteria is met. The calibration parameters of the CRPA are dependent on the location of each antenna element within the array as well as the weighting algorithm that is applied; therefore, different weighting techniques will require different calibration parameters.

In a typical receiver system, each weighted signal is combined and summed to achieve the directional beam pattern, and only one output signal is sent to the receiver [8]. Figure 2.2 below shows the summation process of each antenna element for a single channel receiver. Digital beam forming and null steering can also be implemented using a multi-channel receiver system, where each antenna element is processed across multiple channels simultaneously.

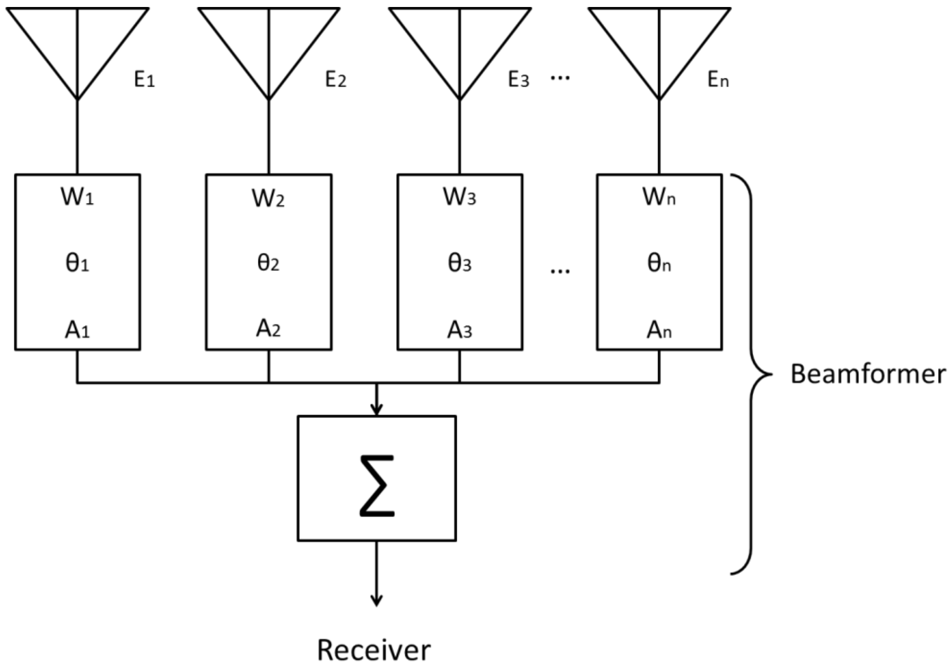

Where:

E – Antenna element

W – Complex Weight

θ – Phase adjustment

A – Amplitude adjustment

Figure 2-2. Weighted signal summation for a single-channel receiver system (adapted from [23]).

2.3 Receiver System

A GPS receiver is a multistage system that determines position and timing estimations from RF signals transmitted by orbiting SVs. Modern GPS receivers consists of analog and digital components that perform the necessary signal conditioning, data sampling, and processing needed to determine the position and timing estimations and remove signal interference, while simultaneously acquiring and tracking multiple SV signals.

In order for the GPS receiver to accurately determine the user's position, the receiver system measures the TOA, Doppler shift, code phase, and carrier phase of the received SV signals [1]. These measurements allow the receiver system to determine the transit time and clock offset of the SV signals, which are used to calculate range estimates. To extract this information, the receiver demodulates the SV signals and estimates the pseudoranges to the orbiting SVs within view. To provide precise position estimations, a GPS receiver will most often rely on carrier phase tracking measurements.

The high frequency carrier phase measurements allow the receiver to determine centimeter-level position accuracy [1]. When implementing carrier phase positioning, the receiver system often resolves the integer ambiguities present in the carrier phase measurements. Unlike the unique structure of the code signal, the carrier signal is a continuous wave signal. A carrier phase measurement, made by the receiver, only determines the partial cycle of the carrier wave signal at the instant the measurement was made. The actual range measurement from the receiver to the transmitted signal is the summation of an unknown number of whole cycles and the partial cycle. The unknown number of whole cycles can be determined through integer ambiguity resolution [1].

The extent of this research is only concerned with the magnitude and phase biases produced by the antenna hardware and receiver system architecture used in a CRPA/SDR system. These antenna induced biases are introduced to the system regardless of the signal acquisition, demodulation, and integer ambiguity resolution technique employed.

Therefore, only signal conditioning and tracking of a continuous carrier wave signal is considered. Under these considerations only one continuous carrier wave signal is transmitted during testing. There is no data modulation on the continuous carrier wave signal; therefore code acquisition and data demodulation are not required.

To determine the magnitude and carrier phase biases produced by the CRPA and receiver system, the test signal is sent through the receiver antenna and RF front-end, where it will be amplified, filtered, down-converted, and sampled by the analog-to-digital converter (ADC), then processed by the receivers baseband processor. The magnitude and carrier phase biases measured by the receiver's baseband processor can be used to determine the calibration parameters and antenna pattern characterization for the CRPA/SDR system.

2.3.1 Digital Receiver Front-End

A single antenna element digital GPS receiver system is presented in Figure 2-3 below [27]. The receiver system consists of the antenna hardware, receiver front-end components, reference oscillator, 12-bit ADC, as well as the baseband and receiver measurement processors. The antenna receives the incoming RF signals transmitted by the orbiting SVs and sends this information to the front-end components of the receiver system. The receiver's front-end components perform signal condition by amplifying, filtering, and down-converting the analog signal to the intermediate frequency (IF). The analog IF signal is then sent to the ADC where discrete digital samples are measured and sent to multiple channels of the digital receiver. To control the gain of the down-convert, the output of the ADC passes through an automatic gain control function (AGC) and is feed back to the down-converter. The baseband processor performs signal acquisition and tracking while the receiver measurement processor determines the pseudoranges and position estimates of the users' location. The baseband and navigation processing is done across all channels of the digital receiver simultaneously, when implementing a SDR receiver architecture, the baseband and navigation processing can be done using embedded software within the receiver or during post processing.

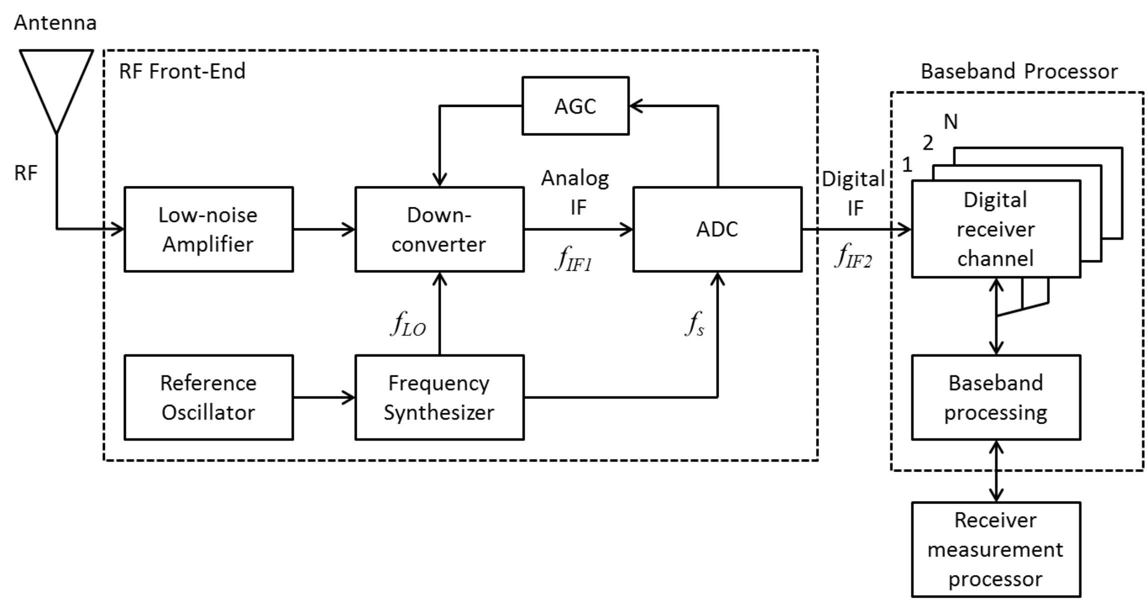

Figure 2-3. Digital GPS receiver system (adapted from [27]).

A receiver system will typically contain a reference oscillator and frequency synthesizer within the receivers RF front-end. The frequency synthesizer uses the reference oscillator to generate a sinusoid signal which is used to down-convert the high frequency RF signal to the IF. Down-converting the RF signal to IF will reduce system complexity and improve measurement accuracy [28]. If the RF signal was not down-converted to IF and direct conversion was implemented, then the receiver's front-end components could introduce unwanted oscillations and single leakage back through the system, potentially introducing signal compression or harmonic distortion into the system [1].

Down-converting the received signal to IF is done through signal mixing. Signal mixing is performed by multiplying the received signal with a reference signal generated using the frequency synthesizers' local oscillators (LOs). If the received signal has a frequency of f_{L1}, then the LO has a frequency equal to f_{L1} - f_{IF}. Depending on the receiver system architecture the IF signal will pass through multiple amplifiers and filters to adequately condition the signal and remove image frequencies generated as a result of the mixing process.

After the signal has been down-converted to an analog IF, it is sent to an ADC, which samples the analog IF signal to produce digital voltage samples. The time-varying voltages are averaged and stored during the sample period. The ADC contains a quantizer which converts the stored voltage samples into digital numbers dependent of the receiver's reference voltage [27]. The ADC performs bandpass sampling on the signal and typically implements a uniform sampling rate. To avoid aliasing the uniform sample rate, f_s, must meet the criteria expressed in equations 2 – 1 and 2 – 2 [29].

$$\frac{2f_H}{n} \leq f_s \leq \frac{2f_L}{n-1} \qquad 2 - 1$$

where n is given by

$$1 \leq n \leq \left\lfloor \frac{f_H}{B} \right\rfloor \quad \text{2 - 2}$$

where:

f_H – High band limit

f_L – Low band limit

B – Signal bandwidth

f_s – Sampling rate

2.3.2 Multi-Channel Receiver System

A multi-channel receiver system, using a combined CRPA/SDR receiver system, will capture the output of each antenna element separately. This allows the receiver to perform digital baseband processing on each channel independently, providing multi-element antenna characterization to process each SV signal independently. The information provided on each channel can be used to implement beam forming and/or null steering techniques to remove unwanted interference and provide anti-jamming capabilities.

Implementation of a multi-channel SDR receiver system increases the complexity and computational requirements of the receiver. Unlike a single-channel receiver system, a multi-channel receiver system must perform the amplification, filtering, down-conversion, digital sampling, and signal processing across all channels in parallel. The increased complexity requires careful consideration when designing the SDR receiver architecture.

The antenna hardware, receiver front-end components, and adaptive algorithms introduce phase variations and induced measurement biases to a CRPA/SDR system. To accurately measure the code and carrier phases of the received SV signals and estimate the user's position, these induced biases must be corrected. This can be done through antenna calibration by determining a complete antenna manifold for each element of the CRPA array. The term manifold is often used in phased array antennas to describe the amplitude and phase variations of the array, as a function of the spatial coordinates. Chapter 3 details the cause of the induced measurement biases, provides an overview of antenna calibration procedures, discusses other calibration approaches for a CRPA system, and presents the calibration method for a CRPA/SDR configuration demonstrated in this thesis.

CHAPTER 3 CRPA INDUCED BIASES AND ANTENNA CALIBRATION

A receiver system implementing a CRPA configuration introduces signal distortion and noise to the system resulting in induced measurement biases. Many factors contribute to the induced measurement biases, such as, the receiver's front-end analog components, the antenna elements comprising the CRPA array, the adaptive processing algorithms used to perform beam forming and/or null steering, as well as the environment in which the receiver system is operating in. To reduce the effects of these biases, the CRPA receiver system must be calibrated.

A variety of calibration techniques can be used to determine the calibration corrections that must be applied to the receiver system to reduce measurement bias and provide an accurate user solution [10] [16] [30]. This thesis presents a demonstrated calibration method for a CRPA/SDR configuration using a multi-channel measurement system. This combined CRPA and SDR system configuration will provide multi-antenna element characterization and calibration measurements that can be used to remove carrier phase biases caused by the antenna elements and receiver front-end components for down-stream adaptive signal processing algorithms.

3.1 Induced Measurement Biases

Carrier phase measurements are susceptible to phase delays and measurement biases within the GPS receiver system. Phase delays are a result of biases in the continuous carrier phase measurement accumulating over time. The carrier phase measurement will vary depending on antenna rotation, satellite rotation, and the elevation angle of the received signal [30]. To accurately measure the carrier phase of the transmitted signal, phase variations and measurement biases must be corrected [31].

Measurement biases caused by the FRPA receiver's analog components, correlation processing algorithms, and clock biases are common to all phase measurements and will not affect integer ambiguity resolution [4]. If the receiver configuration has common-mode biases, the error component will not affect the user solution; however, the clock solution will be affected. Biases caused by the receiver's antenna hardware, adaptive filtering algorithms, and interference sources outside of the receiver system are not common to all phase measurements and will differ for each received GPS signal. Non-common-mode biases have a large impact on the integer ambiguity resolution calculations made by the receiver [4], and can lead to an erroneous position estimation.

During calibration, the measurement biases and phase variations caused by the receiver's antenna hardware are determined and corrected. Biases caused by interference outside of the receiver system such as, ionosphere and troposphere delays, multipath, jammers, satellite orbit error, and satellite clock error are resolved using a variety of error mitigation techniques and are not considered during antenna calibration.

3.1.1 Antenna Hardware Induced Phase Biases

For signal element antennas and FPRAs, phase variations can be corrected using standard calibration techniques [16]. However, CRPAs implementing beam forming and/or null steering algorithms require additional consideration when calibrating [24] [6]. The antenna elements comprising a CRPA introduce additional phase variations and delays due to electromagnetic interference and impedance mismatching caused by mutual coupling and fringing effects between elements.

Mutual coupling affects the phase response of each element and is dependent on the spacing and geometrical configuration of the array. The effects of mutual coupling can produce phase response offsets by as much as 20~30 degrees [5] compared to a single antenna element. Fringing effects will also introduce measurement biases to the receiver system. Fringing effects are a result of the antenna element location around the outer parameter of the ground plane. Elements near the edge of the ground plane can have varying electromagnetic effects. The phase biases introduced to the system by fringing effects can result in 20~30 degrees phase difference between reference element and elements near the edge of the ground plane [5].

A signal antenna element will induce measurement biases to the system due to manufacturing constraints and inherent phase variations dependent on the elevation angle of the received signal. In a CRPA array, the biases induced by each element will compound on one another and vary from element to element. Constructive and deconstructive electromagnetic interference, due to mutual coupling and fringing effects, can induce impedance mismatching between the antenna elements of the CRPA. Any impedance mismatch will affect the magnitude and phase response of each element, resulting in an unpredictable antenna pattern. When implementing beam forming and/or null steering algorithms to steer the antenna pattern, errors caused by electromagnetic interference and impedance mismatching can point the beam in the wrong direction [6].

3.1.2 Induced Biases Resulting From CRPA Processing Algorithms

Beam forming and/or null steering implementation is done by adjusting the amplitude and phase of the received signal for each antenna element in the array. Deterministic processing algorithms must know the direction of the received signal and have preexisting knowledge of the necessary phase adjustments needed to point the beam towards that location. Adaptive processing updates in real time and relies on a given criteria to govern the phase adjustments required to steer the beam in the direction that ensures the existing criteria is met. Both types of processing algorithms depend on accurate phase measurements to determine the amount of phase adjustment that must be applied. Phase measurement biases may cause the processing algorithm to apply the wrong adjustment and point the beam in an undesirable direction, resulting in poor signal reception.

Both deterministic and adaptive signal processing algorithms are susceptible to phase variations in the received signal phase measurement. This is due to the fact that as the SV moves over time, the elevation angle at which the transmitted signal is received varies. These phase variations accumulate to produce phase shifts in the carrier-phase measurement. The effects of this can be removed by implementing carrier-smoothed code or through double difference processing in the receiver [32]. In certain system configurations, this is done by using a constant smooth time with the double differencing processing.

CRPAs implementing adaptive beam forming and/or null steering algorithm techniques introduce additional code phase biases in the presence of multiple interference sources [15]. This is due to the fact that the adaptive weighting algorithms depend on the elevation angle of desired signal and the interference locations. The complex weighting algorithm adjusts the applied phase shifts to compensate for the interference sources to steer the beam away and place nulls in the direction of the interferences sources. With a single-channel receiver, the weighted outputs of each antenna element are combined and summed into a single-channel. Any phase bias or signal interference present will also be combined.

In [15], the code phase biases for adaptive Space-Time Adaptive Processing (STAP) algorithms are investigated in the presence of multiple interference sources. The four types of STAP algorithms investigated are: simple power minimization, geometry-based beam forming, manifold-based beam forming, and a reference correlation vector approach. Up to 38 cm code phase biases were present in algorithms that relied on power minimization. Large code phase biases would hinder precise positioning performance. The geometry-based and manifold-based beam forming adaptive algorithms also introduced significant code phase bias, on the order of 25 to 30 cm. The reference correlation vector approach performed well in presences of multiple interference sources with code phase biases within 8 cm. This is because, unlike the other STAP algorithms investigated, the reference correlation vector approach provides both beam forming and null steering and relies on complete knowledge of the antenna manifold [15].

In [7], carrier phase measurement errors are investigated for various adaptive processing algorithms under both benign and jammed interference scenarios. Under unjammed scenarios, geometric beam forming algorithms can introduce large carrier phase error that effect integer ambiguity resolution. The study reaffirms that, to improve performance, amplitude and phase responses for each antenna element must be corrected. Under jamming scenarios the carrier-phase error increases, especially as the number of jamming sources "exceeds the spatial degrees of freedom" [32]. The study concludes that, "In general, applications that utilize carrier smoothed code (CSC) accuracy will not be adversely affected by the errors induced by CRPAs such as the ones considered here." It adds that, "Geometric CRPA models will likely be inadequate, but absolute CRPA manifold tables should be able to provide reliable carrier phase measurements." [32]

Adaptive signal processing algorithms can be used to perform beam forming and null steering to mitigate signal interference in the presences of multiple interference sources; however, adaptive algorithms can also introduce measurement biases in the system. To implement STAP and correct for the induced biases caused be the receiver signals, each antenna element of the CRPA must be calibrated [10]. Adaptive algorithms cannot remove all biases produced by the antenna hardware and outside interference caused by jammers without predetermined calibration data for the antennas in the array [6] or a complete knowledge of the array manifold [32].

3.2 Antenna Calibration

To accurately measure the carrier phase of the received satellite signal, the phase delays and measurement biases induced by the antenna and receiver hardware and CRPA processing algorithms must be corrected; this can be achieved using antenna calibration corrections. The National Geodetic Survey (NGS) defines antenna calibration as "the act of determining the point of reception of the GNSS carrier phase signals" [16]. NGS also states that, “The point of reception is not a physically measurable location on the antenna, and the point of reception varies depending upon the direction of the satellite signal being received” [16]; it is also known that the point of reception varies as a function of frequency [30].

For a CRPA array, each antenna element will have a unique point of reception that will vary depending on the direction and frequency of the received signal. To reduce complexity, a single Aperture Reference Point (ARP) is used for the entire CRPA array. The ARP is a physical point on the mounted array that acts as a reference for each antenna element’s point of reception. The phase variations measured by each element during calibration are then translated in reference to the ARP. To calibrate the antenna, the phase variations must be measured as a function of elevation and azimuth angels [30].

Many GPS antennas include a calibration look-up-table that provides phase variation corrections that must be applied to the antenna [18]. In accordance with NGS GNSS Antenna Calibration Policy, “NGS conducts these calibrations as an essential service for the surveying, mapping, and engineering infrastructure of the U.S.” [17]. At the time of this work, the NGS only performs dual-frequency and carrier phase calibrations; single-frequency and code delay are not conducted. A variety of calibration techniques can be used to determine the calibration measurements for a CRPA system. Section 3.2.1 discusses other calibration approaches for CRPAs implementing adaptive processing algorithms, while Section 3.2.2 discusses the calibration approach demonstrated in this thesis.

3.2.1 Other Calibration Approaches

In [10] a researched calibration approach is presented for GNSS adaptive antennas. The approach determines the *in situ,* i.e., in position, antenna manifold for an adaptive antenna array by applying various STAP weights and measuring the phase delays for each antenna element using the cross correlation function. A single antenna element is selected and multiple complex weights are applied, while the complex weights applied to the remaining elements are set to zero. Next, the phase delay is measured at the point in which the cross correlation function is at a maximum. Additional complex weights are applied to the same element and the resulting phase delays are measured and stored. The phase measurements are then used in a set of linear equations to solve for the *in situ* antenna element response. This procedure is performed on each antenna element independently, and repeated over time, to obtain the antenna manifolds for the entire array. It was conclude, that the calibration procedure produced accurate *in situ* antenna manifolds for the GNSS adaptive antennas and that further testing should be performed in a real world environment [10] [33].

3.2.2 Demonstrated Calibration Approach

The objective of the thesis is to present the demonstrated method for the performance characterization of a calibration method for a CRPA and SDR configuration that closely represents the eventual fielded systems. This will provide a method of calibration for an array using a hardware and software CRPA/SDR system. For verification, the calibration data produced by the CRPA/SDR system configuration will be compared with calibration data produced using a traditional CRPA test approach where each individual element of the array is characterized by testing one element at a time and adding a 50Ω load to the elements not under test; the 50Ω load acts as a perfect impedance match to the unused antenna elements. The antenna calibration method implemented for this thesis utilizes Ohio University, School of Electrical Engineering and Computer Science Shielded Antenna Anechoic Chamber to collect range measurements. The same calibration procedure was followed for both the CRPA/SDR multi-channel measurement system and the traditional signal-channel measurement system and is outlined in [30] [3].

To determine the calibration data, amplitude and phase response measurements were collected as a function of elevation and azimuth angle, for both co-polarization and cross-polarization. RHCP amplitude and phase calibration data was determined by combining the co-polarization and cross-polarization complex data using equation 3 – 1.

$$E_{RHCP} = \frac{E_\theta + E_\phi}{\sqrt{2}} \qquad 3 - 1$$

where:

E_θ – co-polarization measurement data

E_ϕ – cross-polarization measurement data

E_{RHCP} – RHCP measurement data

A full measurement scan was performed for all elevation angles from 0 to 180 degrees and for azimuth angles at intervals of 0, 30, 60, 90, 120, and 150 degrees. The phase measurements collected by each antenna element are arbitrary and depend on the distance between the transmitted signal source and the AUT aspect angle, and the time at which the data collection begins. Due to this, a phase offset is present for each antenna element. To compensate for the phase offset, the elevation phase measurements are adjusted by a constant phase value to match the reference elevation phase measurement [30]; the adjustment is made at an incident angle of 0º, where the antenna elements are at boresight to the transmitted signal, and signal reception is at a maximum power level. This calibration method provides antenna manifolds for each antenna element comprising the CRPA as a function of elevation and azimuth angles.

CHAPTER 4 SOFTWARE DEFINED RADIO AND BASEBAND PROCESSING IMPLEMENTATION

Digital GPS receivers can utilize a SDR architecture. A CRPA/SDR receiver configuration is advantageous because it can provide added flexibility for additional associated antenna electronics that are used to perform adaptive processing techniques and error mitigation. With the CRPA/SDR system, the antenna calibration and adaptive processing can be done with embedded signal software. This allows the receiver system to be application specific and easily upgradable. It also allows for multiple processing techniques to be implemented on the same set of data within the embedded software of the receiver system. When paired with a CRPA, a multi-channel CRPA/SDR receiver system can process each antenna element of the array continuously and simultaneously and perform beam forming and/or null steering techniques to remove unwanted multiple interference sources and jammers [13]. This chapter examines the SDR front-end architecture utilized in the demonstrated CRPA/SDR calibration method presented, and provides an overview of digital baseband processing; detailing the various stages of the carrier tracking loop.

4.1 Software Defined Radio - Front-End Architecture

The digital receiver's font-end components and ADC can be implemented within the context of a SDR architecture. The SDR architecture for the CRPA/SDR receiver system utilized in this thesis uses Ohio University's third generation Transform-Domain Instrumentation GNSS Receiver (TRIGR), presented in [34], the TRIGR front-end architecture is shown in Figure 4–1 below. Each antenna element is directly connected to one of the TRIGR front-end unit's four RF inputs through coaxial cable. Two TRIGR RF front-end units were used in parallel to provide for eight RF input channels. The TRIGR front-end module first amplifies the RF signal using a low-noise amplifier (LNA) then passes the signal through a RF band-pass filter (RF-BPF). Next, the signal is sent through the first of two digitally controlled variable gain amplifiers (DVGAs) before down-conversion. After amplification, the RF signal is mixed with the phased-locked oscillator (PLO) generated signal, $f_{LO1,}$ and down-converted to an IF of 70 MHz. The IF signal is sent through a low-pass filter (LPF), amplified again, and then enters the second DVGA. Finally, the IF signal is sent through a second BPF to remove any additional out-of-band interference and noise and the signal enters the 12-bit ADC where discrete digital samples are determined by the TRIGR system [34].

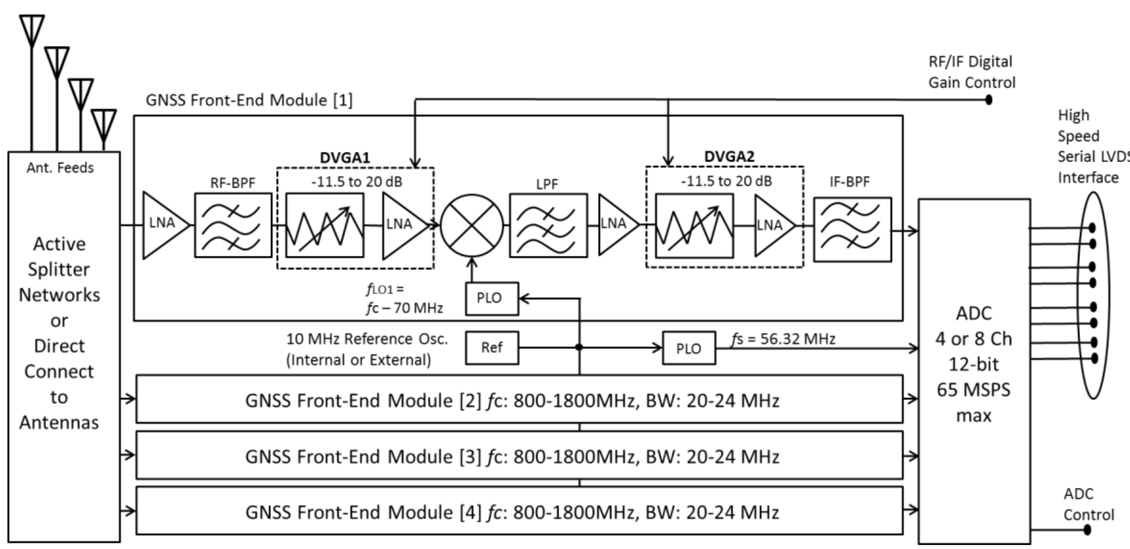

Figure 4-1. TRIGR front-end architecture (adapted from [34]).

The TRIGR system can receive RF signals with a center frequency, f_c, between 800 MHz and 1800 MHz at bandwidths, BW, between 20 – 24 MHz [34]. The system uses a PLO to generate a signal equal to $f_{LO1} = f_c - 70$ MHz, where f_c is the center frequency of the received signal; f_{LO1} is then used by the mixer for down-conversion. For a multi-element CRPA configuration, the phased-locked oscillator (PLO) is attached to either an internal or external reference oscillator to provide a constant carrier phase relationship across all input channels operating at the same frequency. The TRIGR front-end architecture utilizes DVGAs to reduce saturation during amplification of the RF inputs. The DVGAs can be adjusted to reduce sample variance within the system. After the RF signal has passed through the front-end components of the TRIGR system, it is sent to an 8-channel 12-bit ADC converter. The sampling is performed coherently for all channels, with sampling jitter on the order of femtoseconds. The TRIGR system also establishes data integrity checks for every 1ms of data that is sampled. The data integrity verification ensures high-fidelity of the received data samples [34].

The TRIGR front-end module digitizes the downconverted GPS L1 frequency (1575.42 MHz) at a sample rate of f_s = 56.32MHz. The 56.32MHz sample rate produces data streams with digital IFs at 13.68MHz using bandpass sampling [34] [29]. The data streams are sent through a low-voltage differential signaling (LVDS) high-speed serial interface to the TRIGR data collection computer where the digital information is stored to disk for post processing. The TRIGR data collection computer utilizes a field-programmable gate array (FPGA) that performs serial link calibration and verification and the sampled data streams are written to file. During post-processing, baseband processing techniques are implemented to determine the magnitude and phase of each antenna element [34].

4.2 Baseband Processing

The receiver system performs signal acquisition and tracking by cross-correlating the received SV signal with a locally generated replica signal. The phase of the replica signal is adjusted by processing algorithms within the receiver's carrier tracking loop to provide maximum correlation between the desired SV signal and the locally generated replica signal. For this investigation a continuous carrier wave signal was transmitted and no data was modulated onto the signal. The receiver only needs to maintain a continuous lock on the carrier wave signal and track any phase variations exhibited; for further information regarding signal acquisition see [1] [28] [35].

4.2.1 Carrier Tracking Loop

To maintain lock on the received carrier signal, the baseband processor implements a carrier tracking loop. The carrier tracking loop contains the correlator, discriminator, loop filter, and numerically controlled oscillator (NCO) needed to track and maintain lock on the continuous carrier signal. A diagram of the receiver carrier tracking loop is shown in Figure 4–2.

The tracking loop generates a replica signal which is correlated with the sampled IF signal to determine any phase variations or offsets. The replica carrier signal is generated using an NCO, which is dependent on the receiver's nominal frequency, f_{IF}. Correlating the sampled IF signal with the generated replica signal separates the IF signal into in-phase *(I)* and quadrature-phase *(Q)* signal components. The *I* and *Q* components are accumulated over a pre-detecting integration (PDI) time, T_{pdi}, and sent to the phase/frequency discriminator. The discriminator determines the phase/frequency variations of the carrier signal. The output of the discriminator is filtered and feed back to the replica carrier generator where the NCO adjusts the generated replica signal to account for the phase/frequency variations determined by the discriminator. The purpose of the carrier tracking loop is to determine the phase variations between the received signal and the receiver's replica signal and adjust the carrier tracking loop's NCO to match the replica signal with the received signal to ensure that maximum correlation is maintained and the incoming signal can be tracked [28].

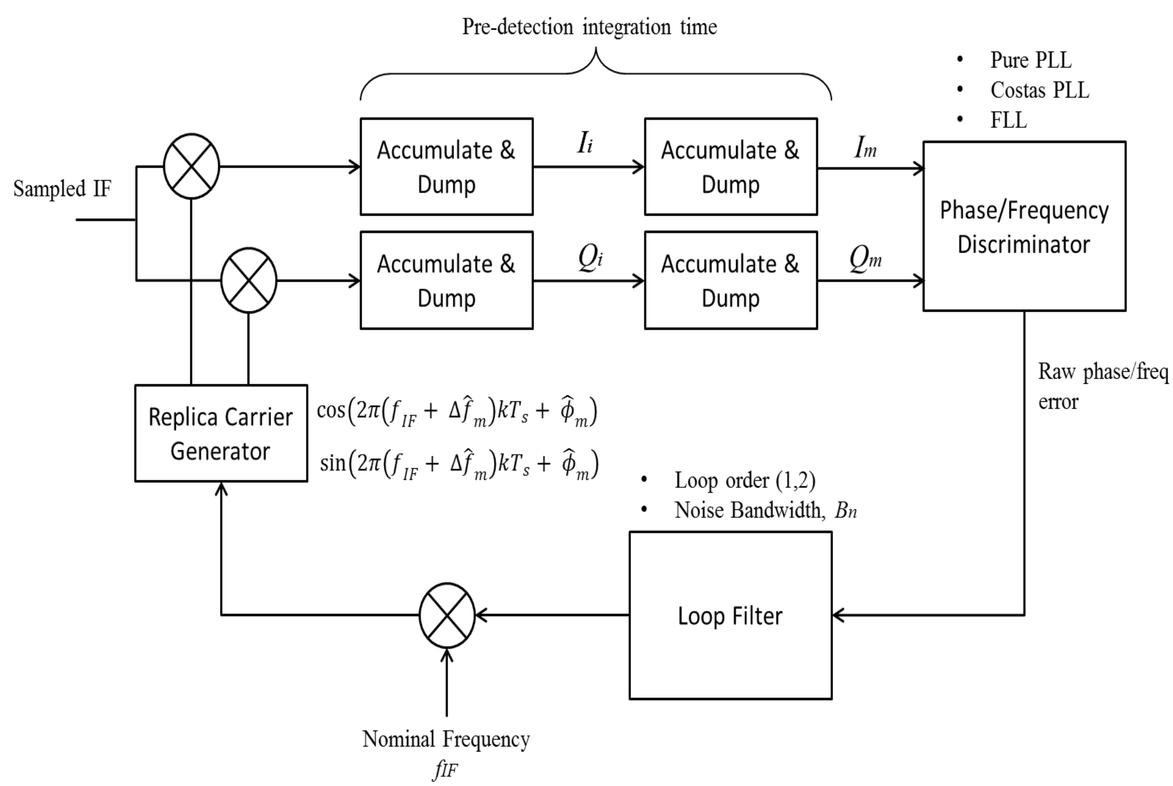

Figure 4-2. Receiver carrier tracking loop (adapted from [27]).

Each component of the carrier tracking loop can be adjusted in the receiver's architecture to provide the best signal tracking performance for the desired application. The PDI time of the correlation function, T_{pdi}, can be varied to maintain smooth phase output estimations. The type of discriminator used is dependent on whether you want to implement a Frequency Locked Loop (FLL) , Phased Lock Loop (PLL), or Costas PLL. The loop filter is dependent on the noise bandwidth, B_n, and the filter order.

4.2.2 Correlator

The first stage in the carrier tracking loop is the correlator. The correlation process performs a windowed low-pass filter that removes the double frequency components of digital mixing. The correlation process compares the similarities between two wave forms and separates the sampled IF signal into its *I* and *Q* components by multiplying the incoming sampled IF signal with a locally generated replica signal and accumulating the results over *N* samples. Equation 4 – 1 [27] expresses the correlation process in discrete time.

$$R(\tau) = \sum_{k=1}^{N} x_{k+\tau} \cdot y_k \qquad 4-1$$

In this equation, $x_{k+\tau}$ represents the sampled signal and y_k expresses the replica signal. The correlation function accumulates across *N* samples, which is determined by the PDI time, T_{pdi}. Increasing the PDI time will accumulate the correlation process over a larger amount of samples, *N*, and can reduce the noise variations of the carrier signal.

Increasing the PDI time by too much however, may cause the correlation function to integrate over an extended period of time, potentially degrading part of the carrier signal's characteristic variations. A larger PDI time has the potential to introduce measurement errors due to cycle slips because the carrier tracking loop has a harder time responding to signal dynamics.

The replica signal generator is controlled by an NCO within the receiver. The NCO generates a waveform based on the desired intermediate frequency, f_{IF}, duration of the accumulator, *N*, and the phase variations determined by the carrier tracking loop discriminator. The *I* and *Q* components of the correlator can be determined from the correlation function using the equations 4 - 2 and 4 - 3 [1] [27].

$$I_{\Delta\hat{f},\hat{\phi},m} = \sum_{k=n+1}^{mN} r_k \cdot \sin\left(2\pi\left(f_{IF} + \Delta\hat{f}_m\right)kT_s + \hat{\phi}_m\right) \qquad 4 - 2$$

$$Q_{\Delta\hat{f},\hat{\phi},m} = \sum_{k=n+1}^{mN} r_k \cdot \cos\left(2\pi\left(f_{IF} + \Delta\hat{f}_m\right)kT_s + \hat{\phi}_m\right) \qquad 4 - 3$$

where:

r_k – received signal

f_{IF} – intermediate frequency

$\Delta\hat{f}_m$ – frequency estimation error

$\hat{\phi}_m$ – phase estimation error

T_s – sample period

The correlation function in the equation above provides the *I* and Q components of the received signal over *N* samples. The received signal, r_k, is multiplied by the cosine and sine terms that represent the replica signal.

The NCO is a mathematical function that generates the replica signal using the sine and cosine mapping functions. The mapping functions are dependent on the intermediate frequency, f_{IF}, the frequency error estimation, $\Delta\hat{f}_m$, the phase error estimation, $\hat{\phi}_m$, and the sample period, T_s. The frequency error estimation and phase error estimation are determined by the carrier tracking loop's discriminator functions. The carrier tracking loop's discriminator estimates the error residuals of the *I* and Q outputs. The estimated error residuals are then passed through the loop filter and sent to the NCO. The NCO uses the phase and/or frequency estimation error residuals to align the replica signal with the received signal phase and/or frequency, respectively to maintain maximum correlation.

4.2.3 Discriminator

Various discriminator algorithms can be implemented to achieve the desired functionality, such as a FLL, PLL, or a Costas PLL. FLL discriminators generate the replica signal based on approximate frequency and are not as sensitive to phase variations as PLLs. FLL discriminators are typically implemented during signal acquisition to estimate the signal frequency, including Doppler, which are less sensitive to dynamic stress; however, for this investigation the AUT remained stationary. Pure PLL and Costas PLL discriminators provide phase variations to the NCO which then adjusts the replica signal depending on these phase variations. Pure PLL discriminators track the full four-quadrant of the input signal, where the Costas PLL tracks the input signal over two-quadrants and can track in the presence of data modulation; because of this, the pure PLL can provide up to a 6 dB improved tracking threshold [27] [28]. For this investigation, the received signal has no navigation data so a pure PLL was selected to determine the phase estimation error residuals.

Pure PLLs determine the output phase error of the carrier signal using a four-quadrant arctangents of the *I* and *Q* components shown in equation 4 - 4 [27].

$$\phi_{err,m} = ATAN2(Q_m, I_m) \qquad 4 - 4$$

The vector magnitude of the carrier signal can also be determined from the *I* and *Q* components, as shown in equation 4 - 5 [27].

$$MAG_m = \sqrt{I_m^2 + Q_m^2} \qquad 4 - 5$$

The phase error, $\phi_{err,m}$, and the vector magnitude, MAG_m, determined by the discriminator, can be used to measure the calibration parameters for the CRPA/SDR system. When the receive system is tested under non-interference scenarios, such as inside an anechoic chamber, the relative phase error and relative magnitude measurements represent the carrier phase and amplitude variations within the receiver system that can be used as a basis for the calibration data. Comparing the phase error and magnitude measurements with true phase and magnitude of the antenna/receiver system will provide the antenna element characterization and calibration parameters of the AUT. The calibration parameters can be used to remove carrier biases caused by the antenna elements and receiver front-end components of the receiver system [10].

Once the phase variations have been determined by the discriminator, the phase error estimates are eventually sent to the NCO. The NCO adjust the generated replica signal to account for the received signals phase variations and maintain maximum correlation between the received and replica signal. The phase error estimates determined by the discriminator may contain measurement noise due to velocity, acceleration, or dynamic stress on the receiver systems as well as thermal noise. To reduce the phase error estimation noise, the output of the discriminator is passed through a loop filter before being sent to the NCO.

4.2.4 Loop Filter

The design parameters for the loop filter are dependent on the noise bandwidth, B_n, and filter order. The loop filter accounts for dynamic stresses in the receiver system by multiplying the input signal by a weighted filter value, dependent on B_n. The output is then fed back into the filter, in closed loop form, to determine an error signal. The output is integrated to remove signal error bias. Higher order loop filter include additional integrators are less sensitive to dynamic stresses such as velocity or acceleration. Figure 4-3 and Figure 4-4 below express first and second order PLL loop filters [27] [28].

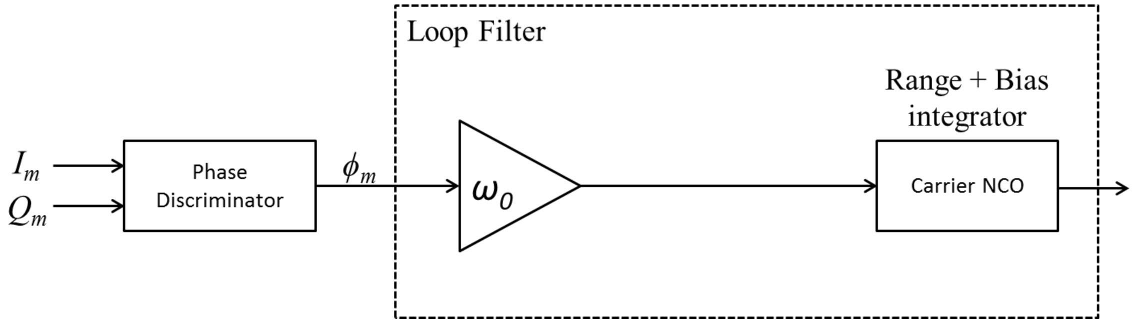

Figure 4-3. First-order PLL filter (adapted from [27]).

$\omega_0 = 4B_n$

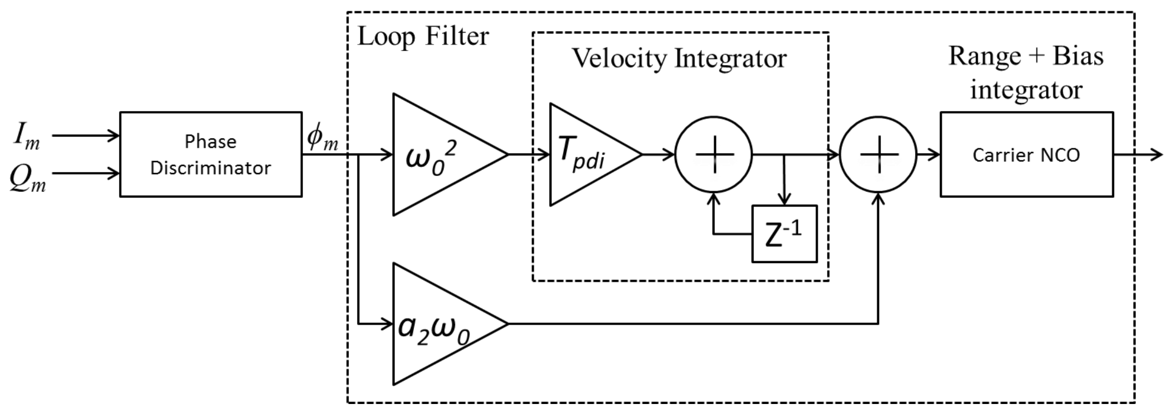

Figure 4-4. Second-order PLL filter adapted from (adapted from [27]).

$\omega_0 = 1.89B_n$

$a_2 = 1.414$

CHAPTER 5 CRPA/SDR CONFIGURATION AND METHOD OF TESTING

A demonstrated method for the performance of a calibration method for a CRPA using a SDR configuration is presented. The objective is to provide a proof of concept for the demonstrated calibration method using a multi-channel CRPA/SDR configuration that closely represents the eventual fielded systems. This chapter discusses the design, construction, and testing of the CRPA/SDR systems used to investigate the CRPA/SDR calibration method. The testing procedure demonstrated provides a method of calibration for an array using a real world CRPA/SDR system. For verification, the calibration data produced by the multi-channel CRPA/SDR system configuration is compared with calibration data produced using a traditional sequential single-channel test approach. For the traditional approach, each element of the CRPA array was characterized individually and 50Ω loads were added to the elements not under test to act as a perfect impedance match to the unused elements.

The AUT for this investigation is a CRPA consisting of 7-active antenna elements, each mounted on a 14.12in circular aluminum ground plane. One reference element was placed in the center of the ground plane, with six outer elements mounted approximately 3.748in (λ/2) from the reference element radially. The elements used were commercially available single feed dual-frequency L1/L2 dual-layer active patch antennas designed by Antcom. Each antenna element is connected to the SDR using a coaxial LMR-195 cable assembly, providing seven channels of data collection. The data collection was performed at Ohio University's School of Electrical Engineering and Computer Science Shielded Antenna Anechoic Chamber located in Morton Hall, Athens, Ohio. This chapter will first present the design parameters and construction of the CRPA and the implementation of the SDR receiver TRIGR system. Next, an overview of the anechoic chamber will be presented. Finally, the traditional sequential single-channel calibration method and the multi-channel CRPA/SDR calibration method will be discussed in detail.

5.1 Hardware Specifications

The antenna elements used for the CRPA are Antcom's active L1/L2 GPS patch antennas, P/N: 1G1215A-XSC-1 [36]. These dual-frequency dual-layer patch antennas are made of 6061-T6 aluminum alloy base and are enclosed in a composite radome with a polyurethane enamel finish. Each active antenna patch element has dimensions 2.080 x 2.080 x 0.690 inches (L x W x H). A SMA female connector is located at the center of the patch antenna and four mounting holes are placed in each corner. The patch antenna elements are right hand circularly polarized (RHCP). Antcom's electrical specifications [36] states that each active patch antenna operates at L1 (1575.42 ± 15.00 MHz) and L2 (1227.60 ± 15.00 MHz) and supports an input impedance of 50 ohms for each frequency. For this investigation the antenna was tested using a continuous carrier wave signal at the L1 frequency. Figures 5.1 – 5.3 illustrate the active patch antenna dimensions for each element [36].

5.1.1 CRPA Design Parameters

The aluminum ground plane used for the CRPA design was fabricated at the Ohio University Engineering Research Machine Lab. The ground plane has a diameter of 14.12in and a width of 3/8in. For the CRPA design, one reference antenna element is mounted to the center of the ground plane and six additional antenna elements are mounted around the reference element in a circular pattern. The six outer antenna elements have different orientation depending on their location on the CRPA ground plane. The outer elements are mounted approximately 3.748in ($\lambda/2$) from the reference element. Figure 5-4 illustrates the ground plane design, element number, and element orientation of the CRPA. Antenna elements 3, 4, 6, and 7 in Figure 5.4 are mounted at a 30 degree offset, ϕ, from the horizontal x-axis; while elements 1, 2, and 5 are mounted in parallel with the vertical z-axis. This provides 60 degrees of separation between each of the six outer elements.

The orientation of each individual element is dependent on the offset, ϕ, and is shown in Figure 5-4. Each antenna element has a center SMA connector and four mounting holes. Each mounting hole is a distance of 0.756in horizontally and 0.756in vertically from the SMA connector. A 1in diameter hole is cut through the ground plane for each element's SMA connector, (*), at a distance of approximately 3.748in from the center of the ground plane. The location of element 2's SMA connector is at a distance of 3.246in in the horizontal x-axis and 1.874in in the vertical z-axis, shown in Figure 5-4.

Each of the seven Antcom active antenna elements are mounted to the circular ground plane and the CRPA calibration testing was performed at Ohio University's School of Electrical Engineering and Computer Science Shielded Antenna Anechoic Chamber. The antenna element numbering and orientation illustrated in Figure 5-4 is facing the backside of the CRPA array as if it were mounted for testing. The viewpoint of Figure 5-1 is at an elevation angle of -90 degrees behind the CRPA, directly on the y-axis. Pictured in Figure 5-2 is the front-side of the constructed CRPA mounted for testing in the anechoic chamber.

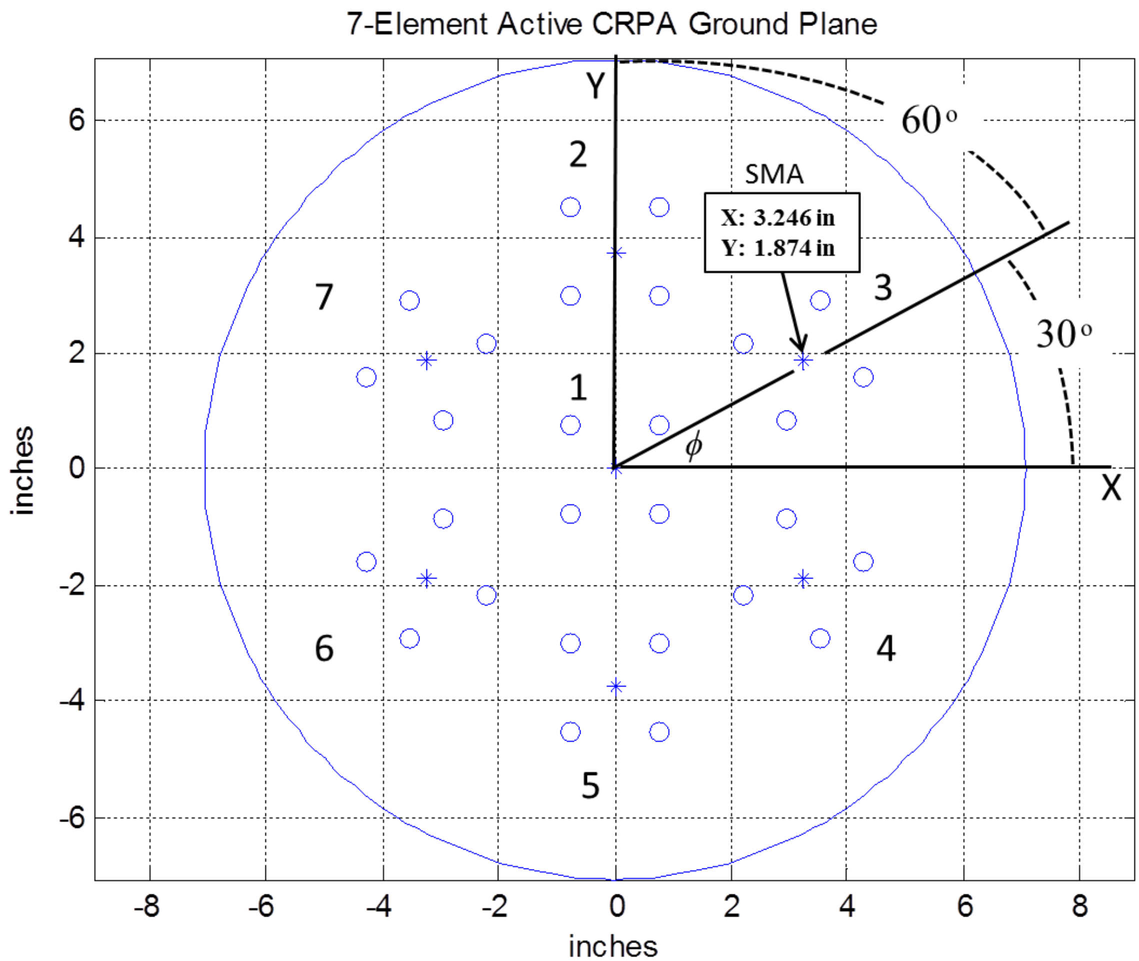

Figure 5-1. 7-Element CRPA ground plane and element locations, back-view, z-axis coming out of the page.

Figure 5-2. Front-view of fabricated CRPA mounted for testing.

5.2 Anechoic Chamber

The calibration testing was performed at Ohio University's Antenna Anechoic Chamber located in Athens, Ohio. The inner walls of the test chamber are shielded with extra-high performance pyramidal microwave absorber that isolates the chamber from any outside RF interference and absorbs transmitted signals within the chamber, minimizing multipath and signal reflection. The microwave absorber provides 100 dB of isolation for RF signals in the frequency range of 200 kHz to 10 GHz. The shielded test chamber has a hybrid near-field antenna test system built by Antcom. The test system consists of a scanner, a motion control system, a vector network analyzer, and a personal computer. The test system allows the AUT to be mounted onto a dielectric tower which is attached to the motion control system. The motion control system allows for full 360 degree rotation in the azimuth and elevation plane [3] [37].

Figure 5-3, illustrates the testing procedure for the rotation of the AUT in the elevation plane. The AUT and dielectric tower are mounted to a lever arm which is controlled by the motion control system. To test the AUT as a function of elevation angle, the motion control system rotates the lever arm clockwise around the y-axis along the xz-plane, so that both the dielectric tower and AUT rotate around the rotation point and remain in parallel to the y-axis. To test the AUT as a function of azimuth angle, the motion control system rotates the AUT around the y-axis. Pictured in Figure 5-4 is the CRPA mounted to the dielectric tower in the anechoic chamber.

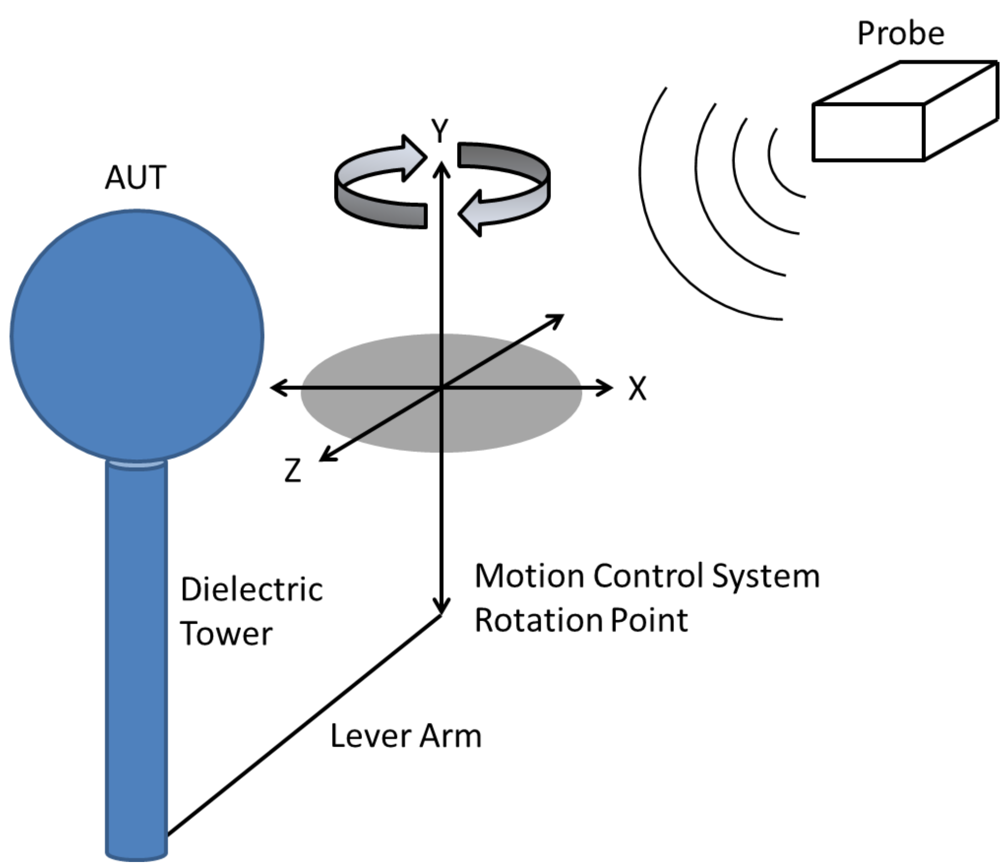

Figure 5-3. Testing procedure as function of elevation angle, AUT rotated clockwise around y-axis along xz-plane.

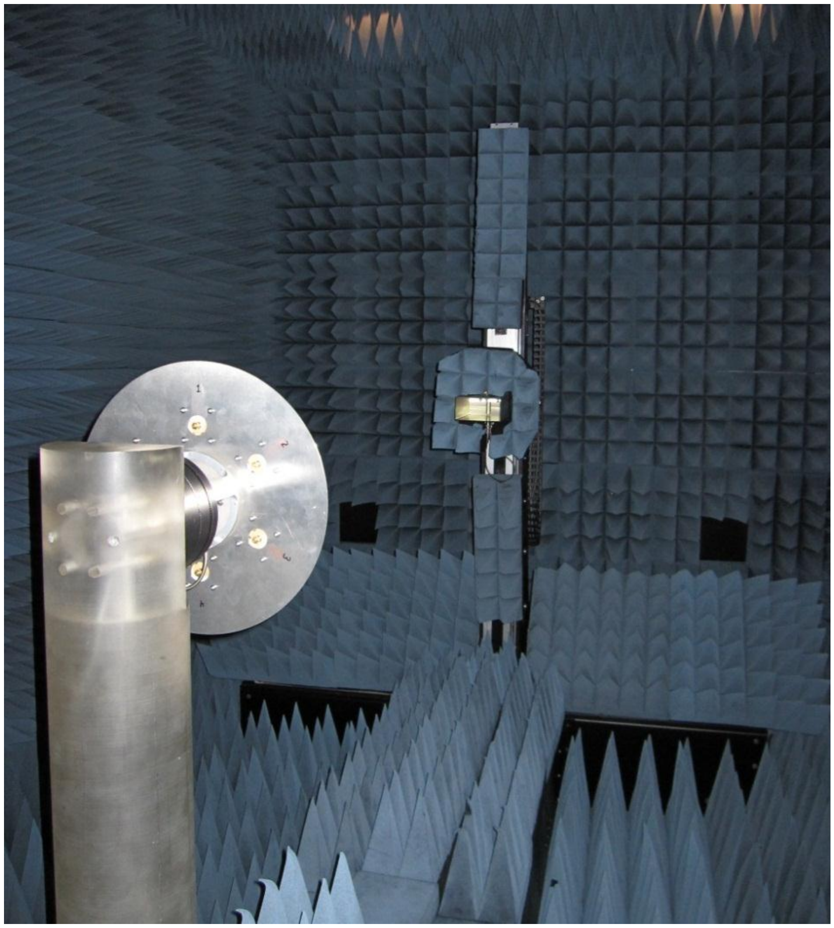

Figure 5-4. CRPA mounted on dielectric tower in anechoic chamber.

Calibration data was collected in two primary modes: 1) Traditional calibration test methods using a single-channel sequential antenna testing technique, and 2) the multi-channel CRPA/SDR combination configuration where the motion base of the antenna system was used but no signal generation or vector network analyzer measurements were used. The traditional calibration method consisted of a single-channel traditional antenna measurement system where one antenna element was tested at a time. The second calibration method implemented the combined CRPA/SDR configuration to provide a multi-channel measurement system.

5.3 Traditional Sequential Single-Channel Measurement System

A traditional calibration testing method was performed using the CRPA and a single-channel traditional measurement system to determine "truth measurements" for the magnitude and phase of each element in the CRPA. Each antenna element was tested separately by connecting one individual element to the vector network analyzer receiver channel and placing 50Ω impedance loads on the remaining elements. The vector network analyzer determined the magnitude and phase measurements of each element over the spatial coordinates. During testing, each AUT element was rotated 360 degrees in elevation and 180 in the azimuth. Each test was also performed using co- and cross-polarization.

To perform the traditional calibration measurements, the vector network analyzer (VNA) generates a test signal at the GPS L1 frequency (1575.42 MHz) based off of its internal reference oscillator. The generated signal output is then transmitted by the waveguide probe. The individual AUT element being tested receives the VNA test signal, transmitted by the probe, and sends the signal to the vector network analyzer receiver channel. The vector network analyzer measures the input signal and determines the signal's magnitude and phase.

To determine the magnitude and phase of the received signal, the vector network analyzer compares the received input signal with its known generated output signal and measures the differences. Once the test scan is complete the vector network analyzer sends the magnitude and phase measurements to a personal computer located outside of the anechoic chamber. Each element of the CRPA is tested sequentially to determine the calibration parameters and antenna characteristics of the entire array over 360 degrees in the elevation plane and 180 degrees in the azimuthal plane. The magnitude and phase measurements determined by the traditional signal-channel measurement system are used as “truth measurements”. The “truth measurements” are compared with the CRPA/SDR multi-channel measurements to provide a basis for comparison and proof of concept validation. The testing setup of the single-channel sequential measurement system is illustrated in Figure 5-5.

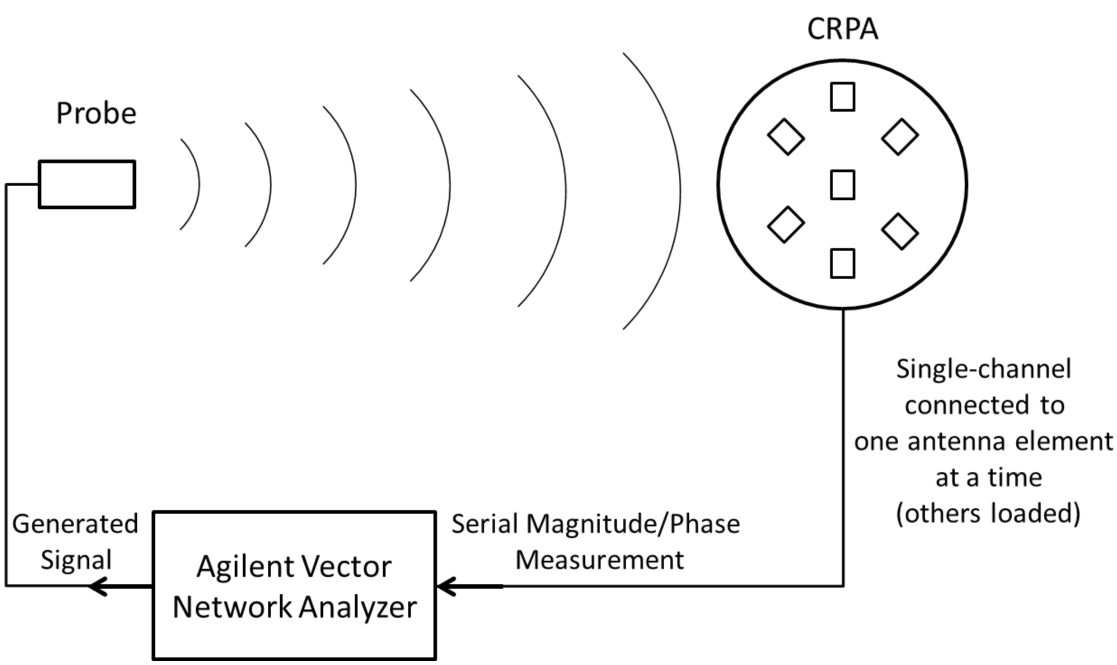

Figure 5-5. Testing setup for single-channel sequential measurement system.

5.4 CRPA/SDR Multi-Channel Measurement System

The objective of the thesis is to present the demonstrated method for the performance characterization of a calibration method for a CRPA and SDR configuration that closely represents the eventual fielded systems. This will provide a method of calibration for an array using a real world CRPA/SDR system. The combination CRPA and SDR system consists of a low-cost 7-element configuration where the antenna RF inputs are feed directly into the multi-channel SDR system. Each antenna element was connected to the SDR RF front-ends using a coaxial LMR-195 cable assembly.

The SDR part of the configuration was implemented utilizing the multi-channel RF-front end and processing capability of the Ohio University SDR. The multi-channel data acquisition system presented uses two synchronized SDR RF front-ends to perform data sampling. Each software receiver channel has four input channels and a local oscillator, allowing the seven signals to be sampled simultaneously. Each software receiver front-end detects the GPS L1 frequency (1575.42 MHz) at a sample rate of 56.32MHz. The 56.32MHz sample rate produce data streams with digital IFs at 13.68MHz. To prevent phase variations due to cable bending, each cable was bundled together inside the dielectric mounting tower. This allowed the AUT to rotate from -90 to 90 degrees in the elevation plane, while minimizing the cable assembly's movement. Due to testing constraints to minimize cable bending, a full 360 degree elevation scan was not achieved.

For the demonstrated calibration method, a carrier wave (CW) signal was generated by an Agilent RF signal generator and phase locked to the SDR's local oscillator. The generated signal was transmitted by the probe and received by the CPRA/SDR measurement system. After the signal is received, the SDR RF front-end components perform the amplification, filtering, down conversion, and analog-to-digital conversion for the receiver system. This setup allows for simultaneous data collection for each of the seven antenna elements of the CRPA. Multiple tests are performed by rotating the AUT across the azimuth and elevation plane. The digital information is stored to disk in the TRIGR data collection computer, and the magnitude and phase measurements are determined in post-processing. The magnitude and phase measurements for the CRPA/SDR system are then compared with the reference "truth" characterization data collected by the traditional sequential single-channel measurement system. Figure 5-6 illustrates the testing setup for the CRPA/SDR multi-channel measurement system.

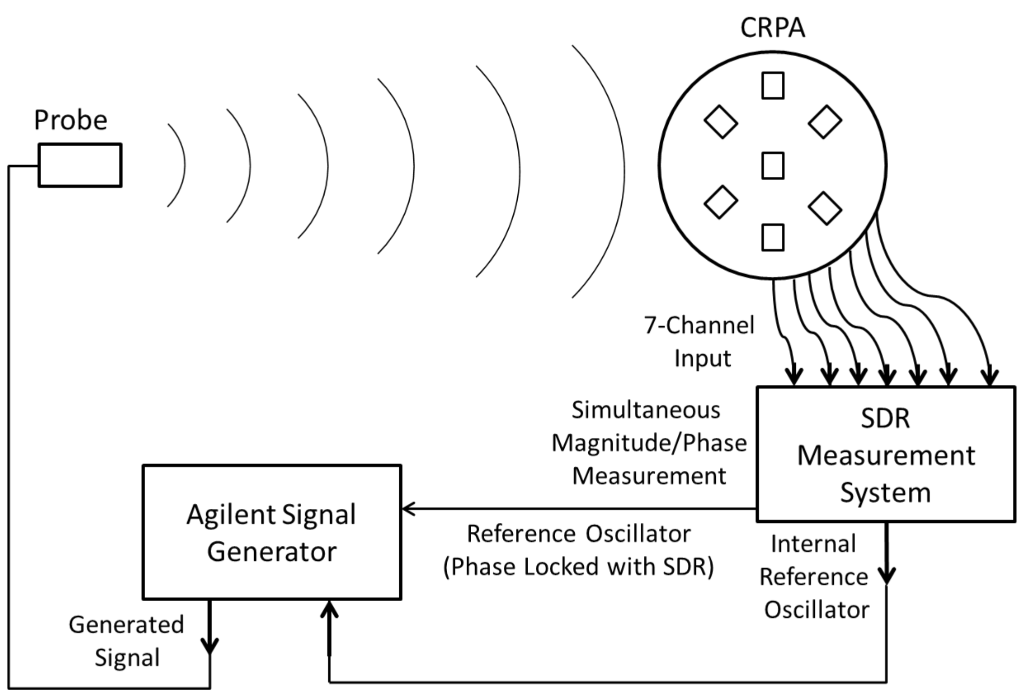

Figure 5-6. Testing setup for the CRPA/SDR multi-channel measurement system.

CHAPTER 6 POST PROCESSING AND CYCLE SLIP RESOLUTION

Utilizing a CRPA/SDR multi-channel measurement system allows RF characterization of each antenna element of the CRPA as well as the SDR receiver system, from the SDR's front-end all the way up to where the signals are digitized. Once the received signals have been digitally sampled by the SDR, the receiver systems can implement signal acquisition, tracking, and error mitigation techniques using imbedded software within the receiver or through post processing. The calibration parameters and characterization of the CRPA/SDR multi-channel measurement systems are determined by measuring the magnitude and phase for each antenna element comprising the CRPA. With a SDR receiver, this process is done through software baseband processing. This chapter discusses the software baseband processing implemented during post processing, detailing the pre-detection integration time and loop filter parameters, as well as, the outlier correction and cycle slip resolution methods used.

6.1 Software Baseband Processing

The measurements made by the SDR are digital representation of the received IF signals for each channel. These digital IF samples are processed by the software baseband processor's NCO, correlator, discriminator, and loop filter across all seven channels simultaneously. The software NCO generates a replica carrier signal vector dependent on the nominal IF frequency (13.68MHz) and sample period, T_s, of the SDR. The digital IF samples are grouped into 1ms data blocks where each data block contains 56320 digital samples.

The digital IF samples are correlated by multiplying the digital samples with the generated replica carrier signal to determine the signal's *I* and *Q* components. The vector multiplication of one sample data block and a replica signal vector accumulates the product of the 56320 samples in each vector, producing one *I* measurement and one *Q* measurement over a 1ms time interval. Following this, another 1ms data block is processed and vector multiplied with the replica signal to produce a second *I* measurement and *Q* measurement, each *I* and *Q* measurement represents 1ms of data. The *I* and *Q* measurements are accumulated over the PDI time, *Tpdi,* before being processed by the carrier tracking loop discriminator.

A PLL discriminator is implemented in software and the magnitude and phase estimations are determined from the accumulated *I* and *Q* data. The phase and magnitude estimations are calculated using equations 4-4 and 4-5 respectively [1] [27]:

$$\phi_{err,m} = ATAN2(Q_m, I_m) \qquad 4 - 4$$

$$MAG_m = \sqrt{I_m^2 + Q_m^2} \qquad 4 - 5$$

The PLL discriminator estimates the residual phase angle between the *I* and *Q* measurements. The phase residual estimation represents the raw phase error of the sampled IF signal. To remove noise, the phase estimations determined by the PLL discriminator are processed by a software loop filter before returning to the NCO. The NCO uses the phase residual estimation to adjust the generated replica carrier signal and maintain maximum correlation between the generated replica signal and the digitally sampled IF signal.

The phase variation estimations are determined for each test conducted; this provides phase and magnitude characterization of the CRPA/SDR receiver system as a function of elevation and/or azimuth. To determine RHCP magnitude and phase characterization, the co-polarization and cross-polarization complex data measurements were combined using equation 3 – 1.

$$E_{RHCP} = \frac{E_\theta + E_\phi}{\sqrt{2}} \qquad 3-1$$

$$E_\theta = I_\theta + jQ_\theta \qquad 3-2$$

$$E_\phi = I_\phi + jQ_\phi \qquad 3-3$$

where:

E_θ – co-polarization measurement data

E_ϕ – cross-polarization measurement data

E_{RHCP} – RHCP measurement data

I_θ – co-polarization in-phase component

Q_θ – co-polarization quadrature-phase components

I_θ – cross-polarization in-phase component

Q_θ – cross-polarization quadrature-phase components

6.2 Pre-Detection Integration Time and Loop Filter Parameters

To remove measurement noise and improve signal quality, the PDI time, *Tpdi*, and loop filter parameters can be adjusted within the software baseband processor. Increasing the PDI time can remove measurement noise while maintaining the signals characteristic qualities; whereas, implementing a loop filter can reduce the systems susceptibility to dynamic stresses allowing the receiver to maintain lock on the incoming signal during the dynamics.

6.2.1 Pre-Detection Integration Time

The PDI time of the software correlator can be adjusted to vary the accumulation time of the I and Q measurements. Increasing the PDI time will average the measurements over a longer time interval and reduce large variations in the measurements; this produces a smoother result with less deviations and increases SNR which is needed at lower elevations angles. However, a very large PDI (e.g., 100ms) time may cause the correlator to average the measurements more than desired and reduce desired characteristic variations the signal might exhibit. When performing antenna characterization, these small measurement variations may provide a more accurate representation of the biases within the system that need to be accounted for when calibrating.

Figures 6-1, 6-2, and 6-3 illustrate the phase estimations for antenna element #1, the reference element, with various PDI times taken over the same arbitrary 5 second data segment. Figure 6-1 shows the phase estimations using a 5ms PDI time, producing 1000 samples over the 5 second data segment. Figure 6-2 shows the phase variations using a

20ms PDI time, with 250 samples. Figure 6-3 shows the results for a PDI time of 100ms, with 50 total samples

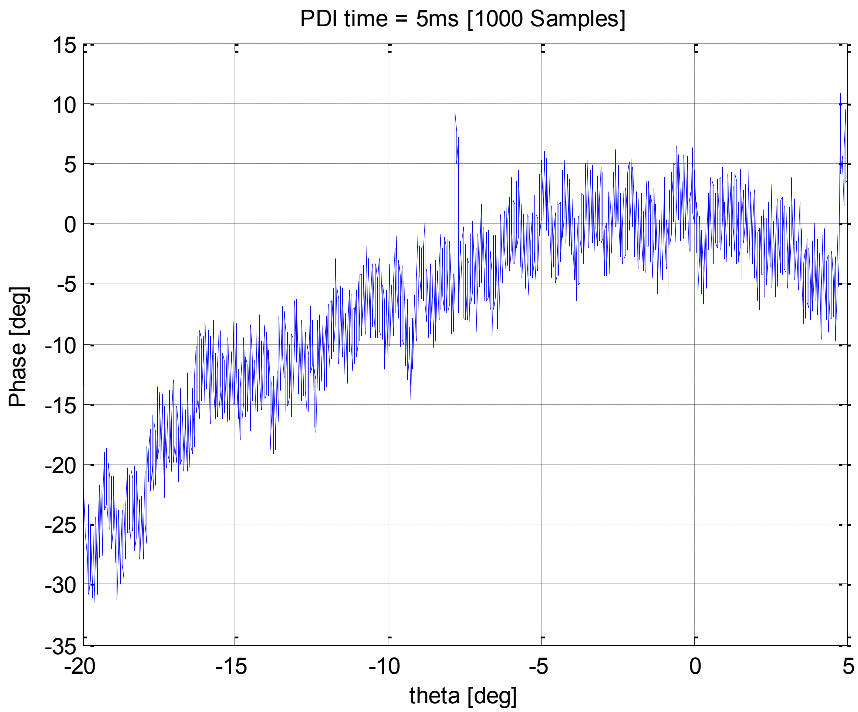

Figure 6-1. Phase estimations over 5 second data set with 5ms PDI time.

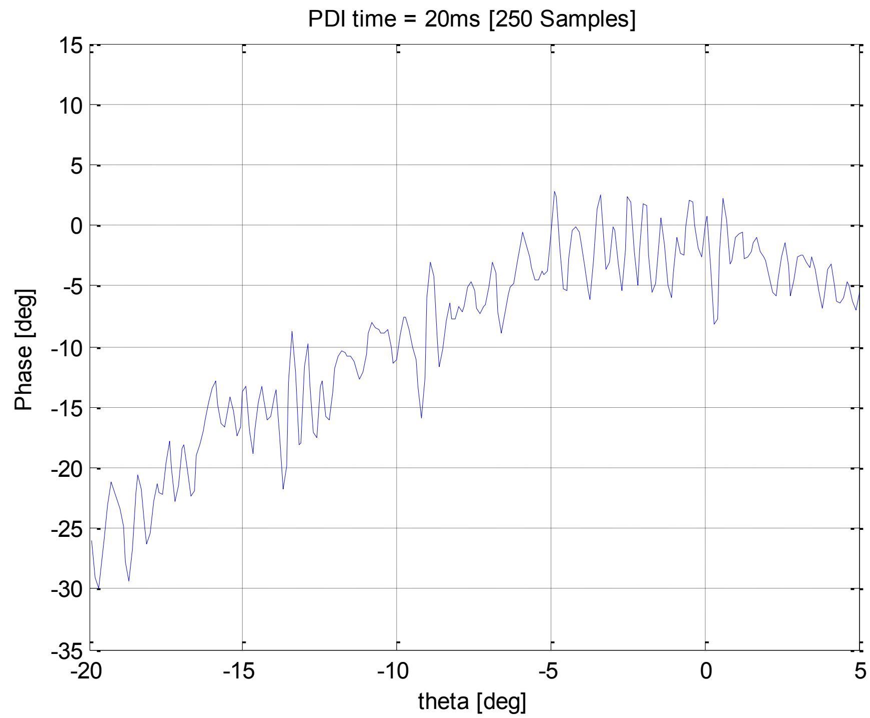

Figure 6-2. Phase estimations over 5 second data set with 20ms PDI time.

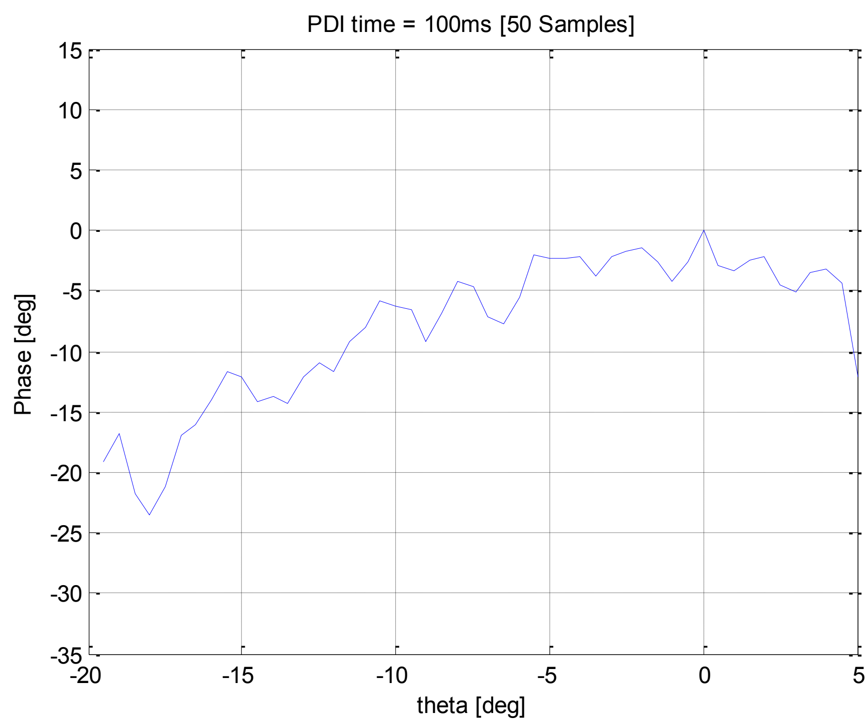

Figure 6-3. Phase estimations over 5 second data set with 100ms PDI time.

The results in Figure 6-1 show a phase characterization with a great deal of variation, while the results in Figure 6-2 exhibit a much smoother phase characterization when compared to the 5ms PDI time; however, by normalizing these results over a larger time interval the phase estimations do not display the same characteristics. The phase estimations for the 5ms PDI time exhibit larger variation and phase spikes throughout the 5 second data segment, whereas with the 20ms PDI time, the larger phase spikes are not as prevalent and the variations are smoother due to the fewer number of data samples. This presents distinguishable phase variation estimations between the two PDI times. This is evident at the end of the data set where the phase estimation for the 5ms PDI time averages around 5°, while the phase estimation for the 20ms PDI time averages around -5°. The phase estimations in Figure 6-3 do not exhibit the large variations present in Figures 6-1 and 6-2 or the phase spikes, and the phase variations are much smaller in comparison. As a result of this, the phase estimation at the end of the data set averages around -10°.

A larger PDI time averages the phase measurements and reduces the characteristic phase spike and variations. To determine the appropriate PDI time for calibration, various PDI times were tested and the results were compared with the “truth” measurements from the traditional calibration method; the PDI time that produced the most accurate results in comparison was then used. It was determined that a 10ms PDI time produced the most accurate results, and was therefore used to calculate the results presented in this thesis.

6.2.2 Loop Filter Parameters

To reduce noise, the raw phase measurements are processed by the software loop filter before returning to the software NCO. A 1st order loop filter removes noise but is sensitive to velocity stresses; whereas, a 2nd order loop filter is insensitive to sudden velocity changes but sensitive to acceleration stresses [27]. The performance of the loop filter is defined by the noise bandwidth, *Bn.* The greater the noise bandwidth, the larger the amount of allowable noise to pass through the filter. Typically, a narrower noise bandwidth provides better performance during calibration.

The testing system for the chamber calibrations consisted of the AUT and dielectric tower mounted to a lever arm. To test the AUT as a function of elevation angle, a motion control system rotates the lever arm clockwise around the probe, so that both the dielectric tower and AUT rotate around the same rotation point. The dynamics of this system provide a constant velocity during testing, therefore, a 1st order loop filter was implemented to remove noise in the phase estimations. A 2nd order loop filter was also implemented; however, the results were nearly identical to the 1st order phase estimation because the testing setup did not produce sudden velocity stresses. Figure 6-4 and 6-5 show the results over the same 5 second data set with a 5 millisecond PDI time using a 1st order filter with a 10 Hz noise bandwidth, and a 1st order filter with a 1 Hz noise bandwidth, respectively.

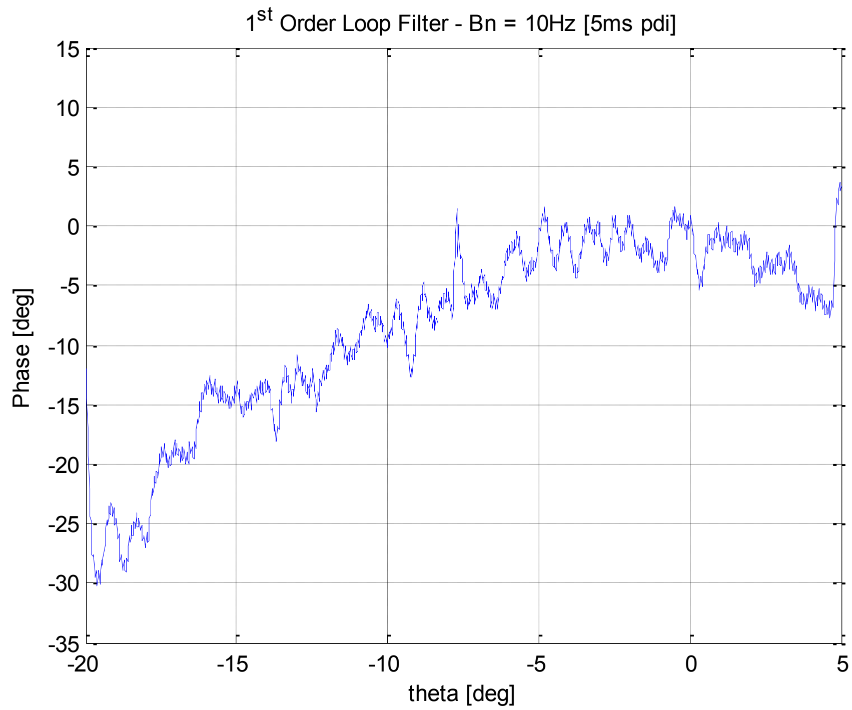

Figure 6-4. Phase estimations over 5 second data using a 1st order loop filter, Bn = 10Hz.

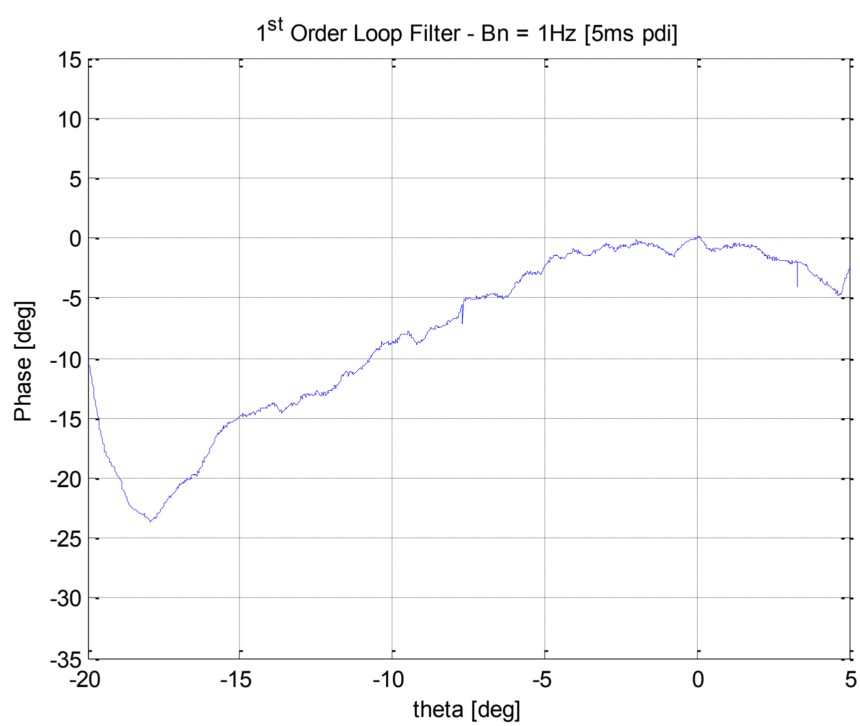

Figure 6-5. Phase estimations over 5 second data using a 1st order loop filter, Bn = 1Hz.

Figure 6-4 illustrates the phase estimations for a 1st order loop filter, with *Bn* = 10 Hz. The loop filter removes a large amount of noise and produces much smoother results with nearly the same characteristic phase pattern. Figure 6-5 shows the phase estimations for a 1st order loop filter, with *Bn* = 1 Hz. The narrower noise bandwidth reduces the amount noise that is allowed to pass through the filter and produces smoother phase estimations with less variation.

A larger PDI time will normalize the phase residual estimations while the loop filter removes signal spikes caused by dynamic stresses in the receiver system. These processes will reduce measurement noise in the system; however, they may also reduce characteristic phase variations in the measurement. The phase variations represent the characteristics of the antenna elements in the system, to acquire the most accurate representation, careful consideration must be used to find the best PDI time. To determine the appropriate PDI time and loop filter noise bandwidth, various values were tested and compared with the “truth” measurements of the traditional calibration approach; the values that provided the greatest accuracy were then used.

6.3 Outlier Detection and Cycle Slip Correction

A multi-channel measurement system utilizing a CRPA/SDR receiver system provides high resolution magnitude and phase estimations for the CRPA configuration; however, an occasional outlier may appear in the measurement results. The outliers are a result of drops in the magnitude of the signal. Drops in signal magnitude can cause cycle slips to occur within the PLL of the discriminator and produce large spikes in the phase residual estimations. When the phase residual estimations are accumulated, any outliers in the phase residual measurements will also accumulate and produce erroneous phase estimations. When the co-polarization and cross-polarization phase estimations are combined to form RHCP phase estimations, the phase error will also be combined. Error graphs illustrating the number of phase cycle slips that occurred due to outlier measurements are presented in the Appendix.

The phase residual estimations determined by the PLL represent the phase differences between the NCO's replica signal and the received signal being measured. To maintain maximum correlation, the NCO adjusts the phase of the generated replica signal to match the phase of the received signal. This phase adjustment is dictated by the phase residual estimation determined by the PLL. An outlier measurement will produce a large phase residual between the generated replica signal and received signal. A PLL is sensitive to phase residual errors larger than ±180, due to the four-quadrant arctangent, equation 4 – 4, used to determine the phase residual estimation [27]. If the outlier measurement results in a phase residual error large than ±180, a cycle slip may occur resulting in large variations in the filtered phase estimations. To compensate for this effect, the phase residual estimations can be filtered to determine the location and magnitude of the outlier measurements. This information can be used to correct large phase variations and prevent cycle slips in post processing.

To filter the phase residual estimations and resolve cycle slips, each channel of the data set is processed twice by the software baseband processor in a post processing fashion. This process is illustrated in Figures 6-6 and 6-7 below. During the first iteration, the digital IF signal passes through the correlator, where the digital information is accumulated and dumped, then the magnitude and phase estimations are determined by the PLL discriminator. Following this, the phase difference between the current phase estimation and the previous phase estimation is calculated. This phase difference is then compared with a threshold that is three times the standard deviation, 3σ, of the phase residual estimations. If the phase difference is larger than 3σ, a cycle slip is declared and the sample location and phase difference of the outlier is stored. The standard deviation, σ, is initialized at 0.1 degrees then updated for each consecutive phase residual estimation. This process continues until a cycle slip is declared; once declared, σ is reset to 0.1 degrees and a new σ is determined and updated using the consecutive phase residual estimation calculated after the cycle slip. The entire data segment is processed in this fashion during the first iteration and the unfiltered phase estimations are passed through the loop filter and sent to the NCO to adjust the replica carrier signal. After the first iteration, any phase outliers present have been located and their sample location and magnitude have been stored; however, the magnitude and phase estimations have not been filtered to correct for outliers.

During the second iteration, the data set is once again processed by the software baseband processor's correlator and discriminator to determine the magnitude and phase estimations; however, the software baseband processor uses the stored outlier data to filter the phase estimations and correct for any outliers. This is done by subtracting the outlier's phase difference at each erroneous location so that phase residual estimation is equal to the value before the cycle slip occurred; any phase residual estimation that was within the threshold during the first processing iteration is unaffected. Removing the outliers measurements can affect some of the phase estimations characteristic variations; however, due to the high resolution of the measurements this effect is negligible.

The same process is performed on the magnitude measurements to determine the locations of drops in magnitude. The difference between the current magnitude measurement and the previous magnitude measurement is calculated and compared with a threshold. If the difference is greater than the threshold than the location and difference of the magnitude outlier is stored and removed during the second iteration. Figure 6-6 below illustrates the cycle slip resolution processing performed. A flow chart showing the outlier detection and correction processing is presented in Figure 6-7.

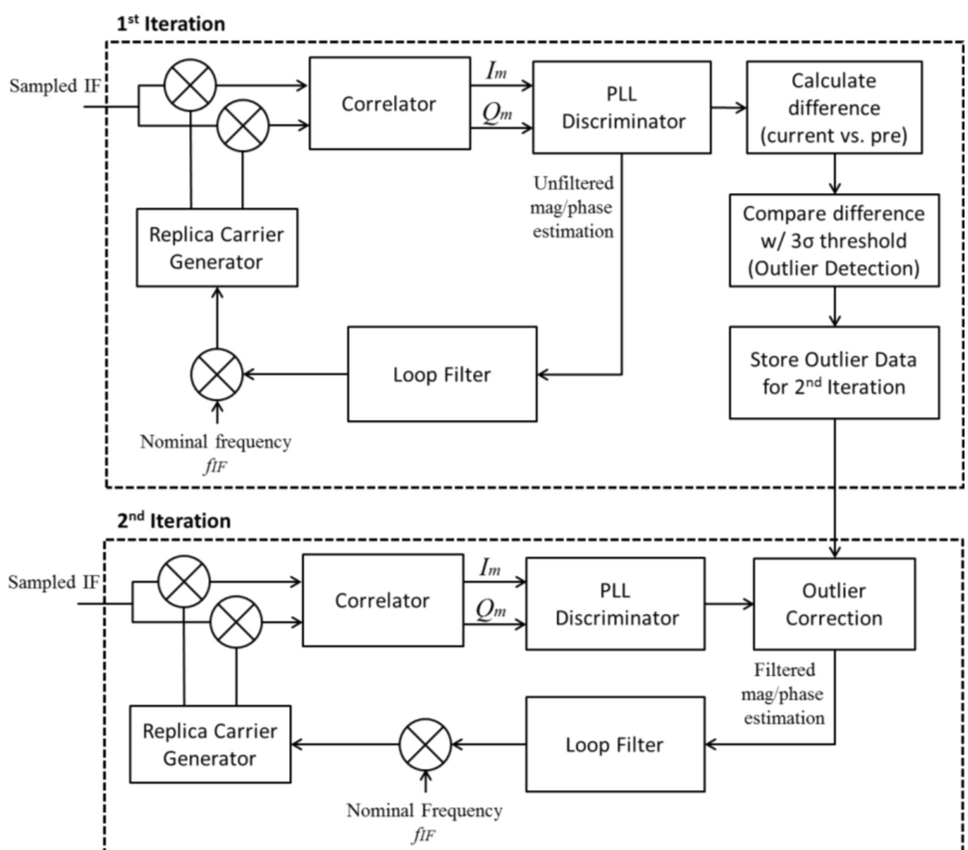

Figure 6-6. Cycle slip resolution processing.

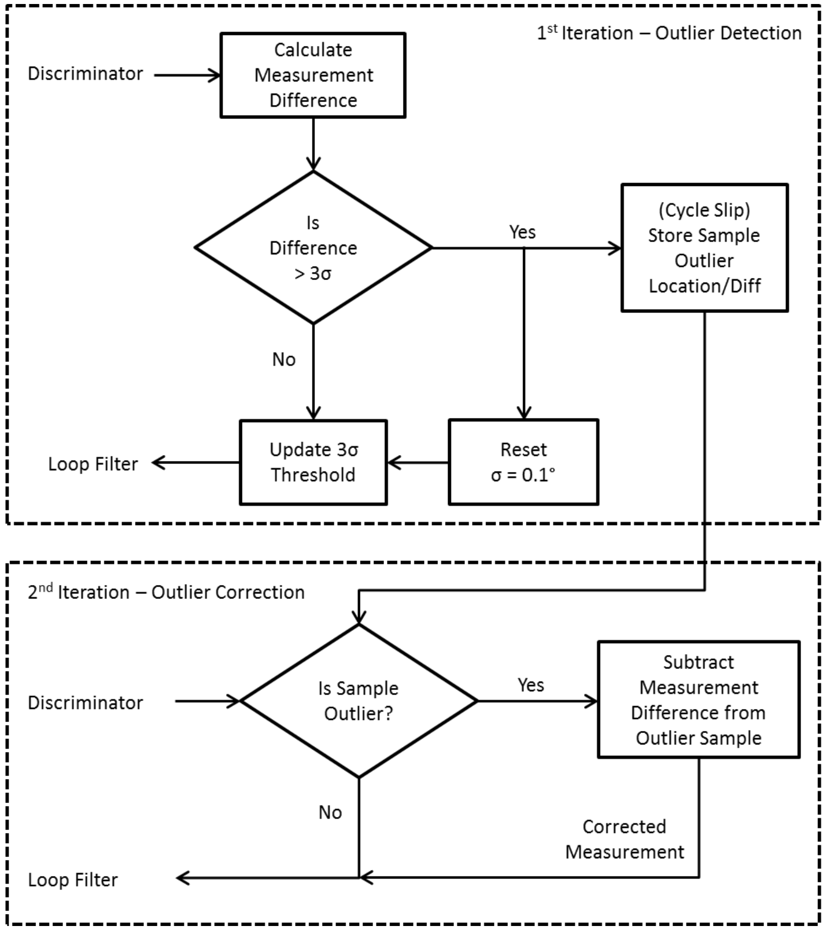

Figure 6-7. Flow Chart of Outlier Detection and Correction.

To illustrate the performance of the outlier detection and cycle slip correction technique, a sample data set was processed from the reference antenna element #1, over 5 seconds. Figure 6-8 shows phase differences between the consecutive unfiltered phase residual estimations for both co-polarization and cross-polarization; as well as, the 3σ threshold. This data set was calculated during the first iteration of software baseband processing. Figure 6-9 illustrates the filtered phase difference after the outliers have been removed during the second processing iteration. Outliers in the phase residual estimation measurement result in large phase differences.

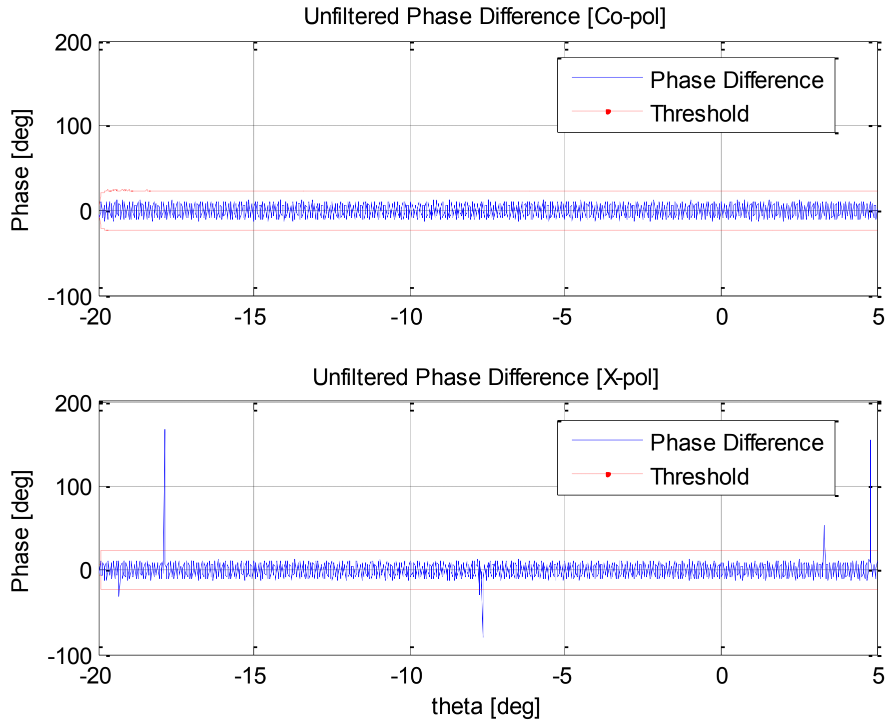

Figure 6-8. Co-pol and X-pol phase differences, unfiltered phase residual estimations and 3σ threshold.

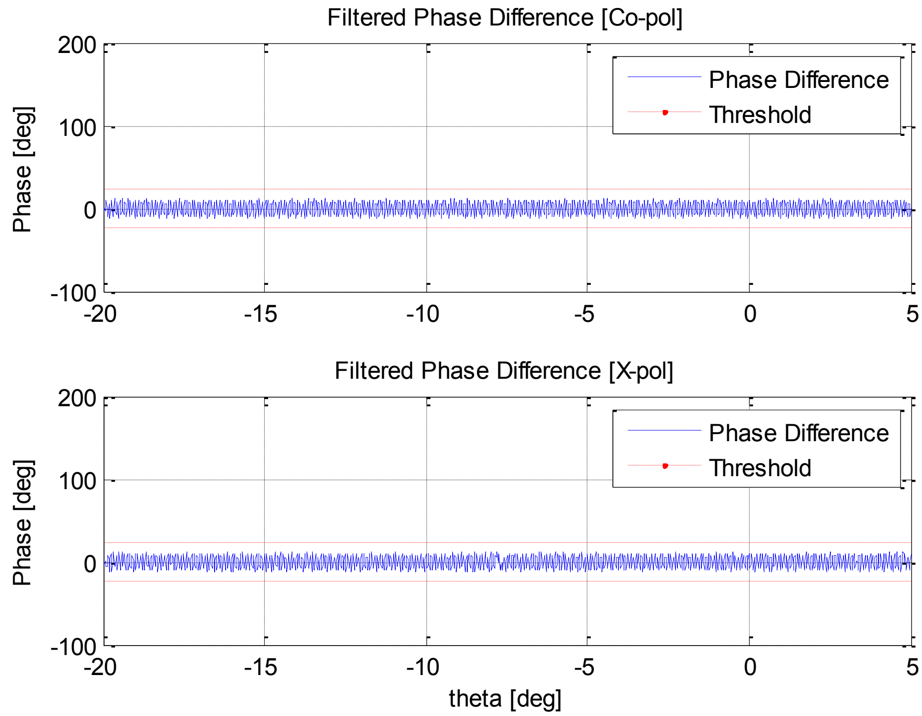

Figure 6-9. Co-pol and X-pol phase differences, filtered phase residual estimations and 3σ threshold.

In Figure 6-8 outliers are present in the cross-polarization data set where the phase difference is larger than the threshold; whereas, no outliers are present in the co-polarization data set for this data set. The location and magnitude of phase differences that exceed the 3σ threshold are stored so that the phase residual estimations can be filtered during the second iteration of the software baseband processing. The results in Figure 6-9 show that the phase residual estimations remain within the 3σ threshold and provide the signal characteristic phase variations.

After the phase differences have been filtered and the outliers removed, the corrected phase residual estimations are sent through the software baseband processor's loop filter and returned to the NCO. Since the outliers have been corrected, the NCO will only adjust the phase of the replica signal by the amount determined by the loop filter.

To determine the calibration parameters and CRPA/SDR characteristic phase variations as a function of elevation and/or azimuth, the filtered co-polarization and cross-polarization phase residual estimations are combined to form RHCP phase residual estimations using equation 3 - 1. The RHCP phase residual estimations are accumulated to provide the elements characteristic calibration parameters. Figure 6-10 illustrates the accumulated unfiltered RHCP phase residual measurements before the outliers have been removed and Figure 6-11 illustrates the accumulated filtered phase residual measurements when the outliers have been removed. The results shown in both Figures 6-10 and 6-11 are for the reference antenna element, element #1, over a 5 second data set.

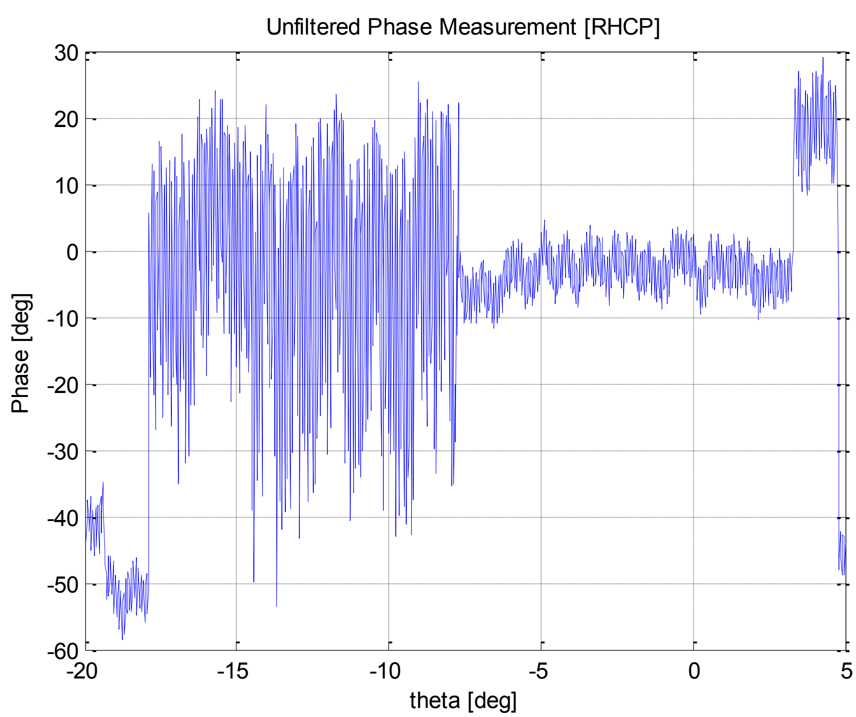

Figure 6-10. Accumulated unfiltered RHCP phase measurement, outliers included.

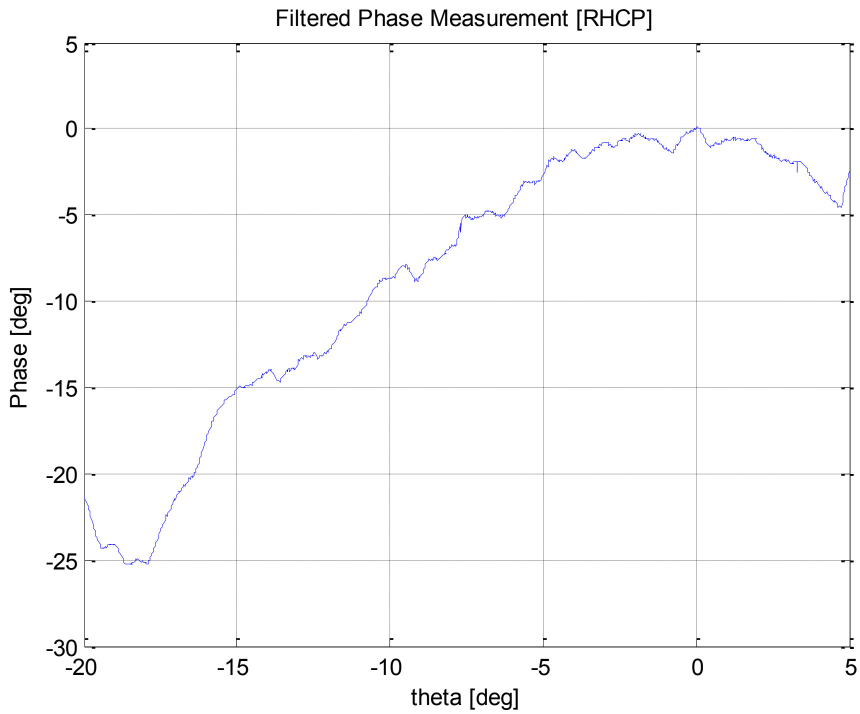

Figure 6-11. Accumulated RHCP filtered phase measurement, outliers removed.

As illustrated in Figure 6-10, if the phase residual estimations are not filtered, large phase differences, caused by the outliers, will accumulate over time resulting in large phase spikes and erroneous phase estimations. Due to the accumulated phase spikes, the erroneous phase estimation for the unfiltered data set are very noisy and do not provide an accurate representation of the elements characteristic phase variations. As shown in Figure 6-11, by filtering the phase residual estimations and setting the outliers to the value before the cycle slip occurred, the accumulated phase measurements do not exhibit large phase spikes and more accurately represents the expected characteristic phase estimations for the CRPA/SDR system.

CHAPTER 7 DATA ANALYSIS

A traditional sequential single-channel calibration test method was first performed using the CRPA to determine "truth measurements" for the magnitude and phase of each element in the CRPA array. Each antenna element was tested separately by connecting one individual element to the vector network analyzer and placing 50Ω impedance loads on the remaining elements. The vector network analyzer determined the magnitude and phase measurements of each element over the spatial. The measurement data was then processed by the Antcom antenna measurement system software to produce antenna radiation patterns. During testing, each AUT element was rotated 180º in elevation and 360º in the azimuth in the anechoic chamber. Each test was also performed using co- and cross-polarization.

The second method, using the same 7-element CRPA and the SDR multi-channel data acquisition system, was then tested in the anechoic chamber. Each antenna element was connected to the SDR RF front-ends using LMR-195 coaxial assemblies. For these demonstration tests, a CW signal was generated by an Agilent RF signal generator, which was phase locked to the SDR receiver system. This setup allowed for simultaneous data collection for each of the seven antenna elements of the CRPA. Multiple tests were performed by rotating the AUT across the azimuth and/or elevation plane and the magnitude and phase measurements where determined in post-processing using MATLAB®.

7.1 CRPA Calibration Testing

The results presented in this section were tested as a function of elevation angle. The elevation measurement data presented here were collected from incident angles of -90º to +90º. The elevation data scans were performed using both the single-channel calibration method and the demonstrated multi-channel calibration method. The data for each calibration method was analyzed separately in post processing and are presented here for comparison and validation.

The phase measurement data collected by each antenna element is arbitrary and depend on the distance between the transmitted signal source and the AUT, and the time at which the data collection begins. Due to this, a phase offset is present for each antenna element. To compensate for the phase offset, the elevation phase measurements are adjusted by a constant phase value to match the reference elevation phase measurement [30]. The adjustment is made at an incident angle of 0º, where the antenna elements are at boresight to the transmitted signal, and signal reception power level is at a maximum. Additionally, the magnitude measurements are adjusted so that the center reference element is 0 dB at an incident angle of 0º; the remaining elements are adjusted accordingly to clearly show the variations in magnitude between elements.

The AUT was tested at an azimuth angle of 30º for both calibration methods, in reference to the CRPA orientation presented in Chapter 5. Figure 7-1 illustrates the orientation and element locations of the AUT for both calibration methods used during testing. The antenna element numbering and orientation illustrated in Figure 7-1 is the backside of the CRPA as if were mounted for testing. The viewpoint of Figure 7-1 is at an elevation angle of 180º behind the CRPA, directly on the z-axis. At this orientation, antenna elements 2, 3, 5, and 6 are oriented at 30 degree offsets from the vertical y-axis.

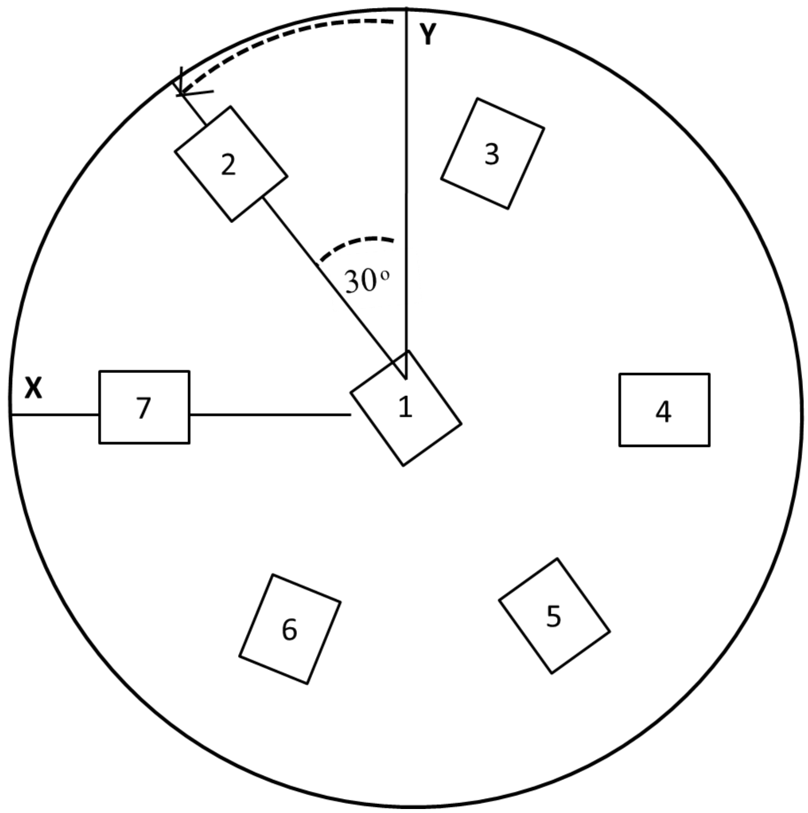

Figure 7-1. 7-Element CRPA element locations at azimuth angle of 30º, viewpoint at an elevation angle of 180º behind the CRPA.

7.2 Results and Discussion

To perform calibration testing as a function of elevation angle, the AUT was rotated 180º around a rotation point in parallel to the y-axis along the xz-plane, starting at an incident angle of -90º and finishing at +90º. With this testing procedure, each antenna element of the CRPA will have relatively the same phase at an incident angle equal to 0º. This is because at zenith, each element will be at boresight to the signal transmitted by the probe were antenna gain is at a maximum. Additionally, because each data set began with measurements at larger incident angles, where received signal power is lower, the software baseband processor was initialized at the center of the data set during post-processing. This initialized the carrier tracking loop at an incident angle of 0º where the antenna gain was at a maximum. To develop a complete antenna manifold across the elevation plan, the data was first processed in the forward direction through the data set, and then processed in the reverse direction through the data set; the data processed in both the forward and reverse directions was then combined to develop the results presented. To process the data in this fashion, the center of the data set, where the AUT was at an incident angle of 0º, was first selected. Next, the data was processed in the forward direction by processing the measurement received at incident angles from 0º to +90º. Then, the data was processed in the reverse direction by selecting samples in reverse order and processing the measurements received at incident angles from 0º to -90º. The data processed in the reverse direction was then flipped from left to right so that the result where continuous when combined with the data processed in the forward direction.

Cycle slip resolution was also implemented during post processing, as described in Section 6.3, to reduce the effects of phase variations caused by drops in amplitude. During post processing, a PDI time of 10ms was used in conjunction with a 1st order loop filter, with a loop bandwidth of B_n = 1Hz. After outlier and cycle slip correction, the magnitude and phase measurement results for both the single-channel and multi-channel calibration methods are presented and compared in Figures 7-2 through 7-19.

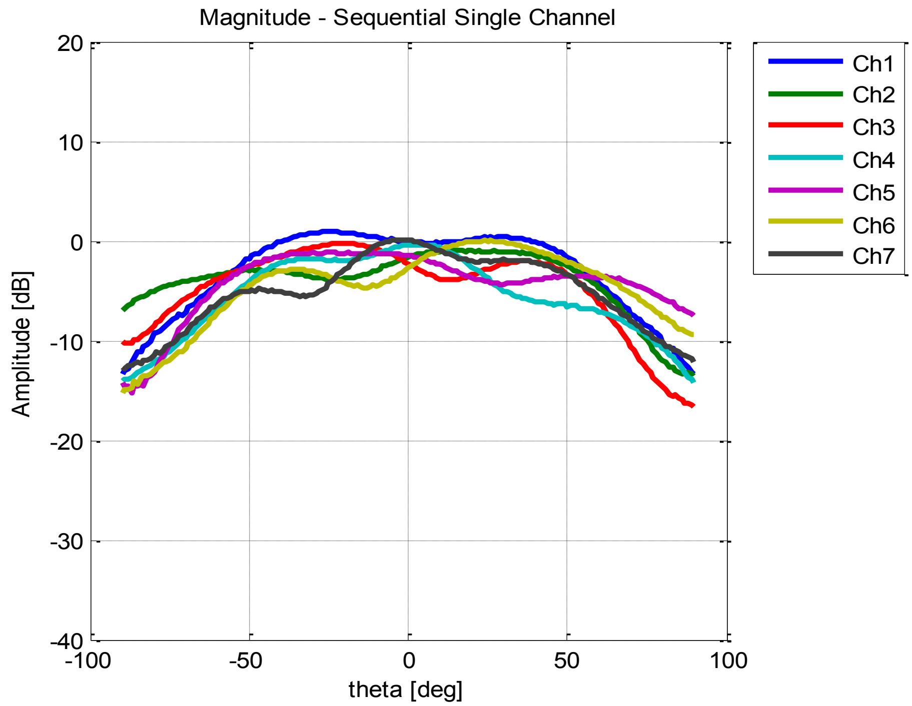

Figure 7-2. Magnitude sequential single-channel calibration method, all channels.

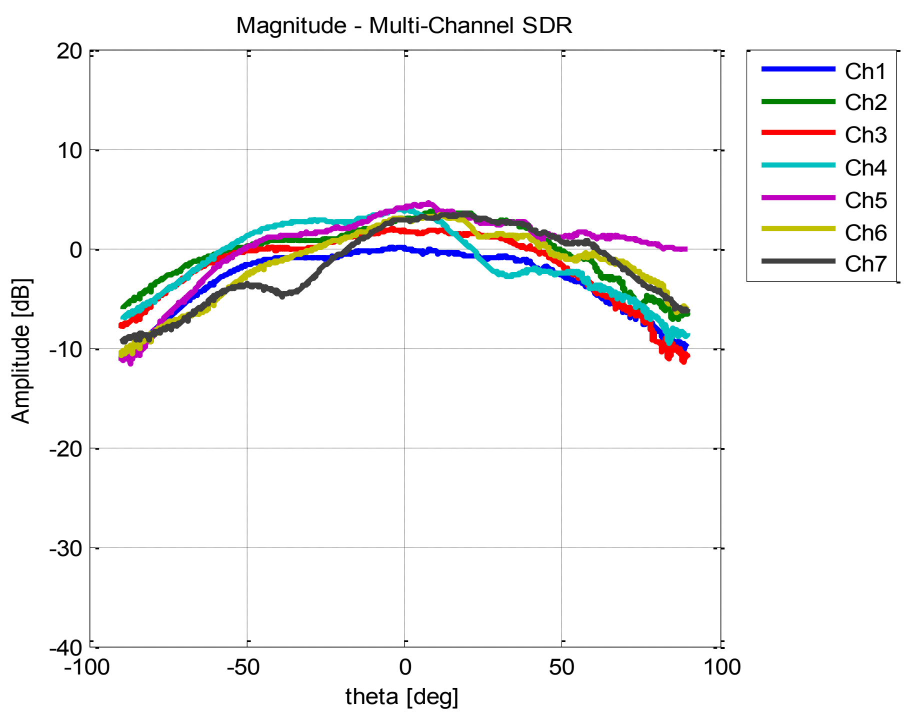

Figure 7-3. Magnitude multi-channel calibration method, all channels.

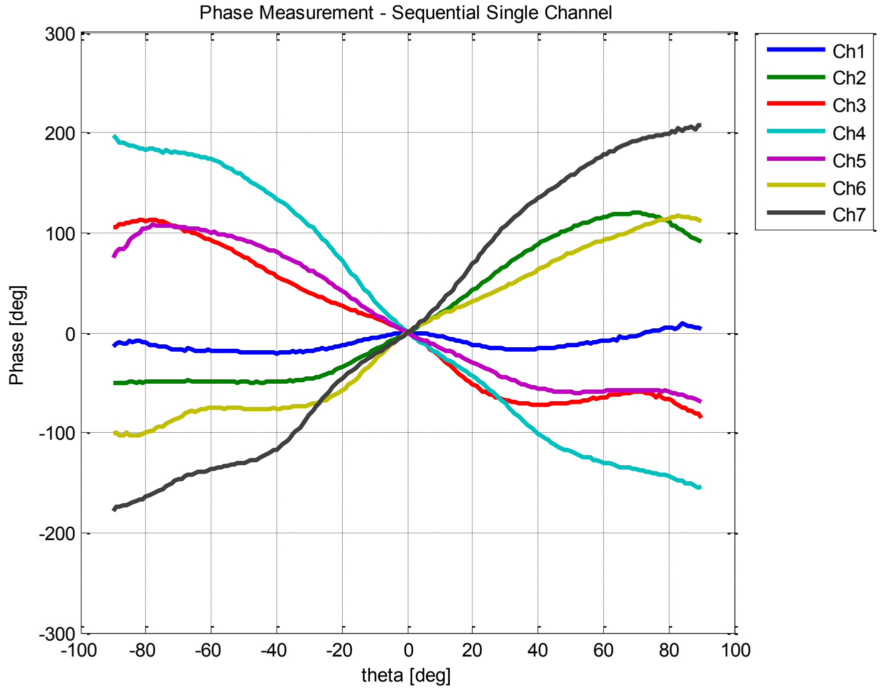

Figure 7-4. Phase sequential single-channel calibration method, all channels.

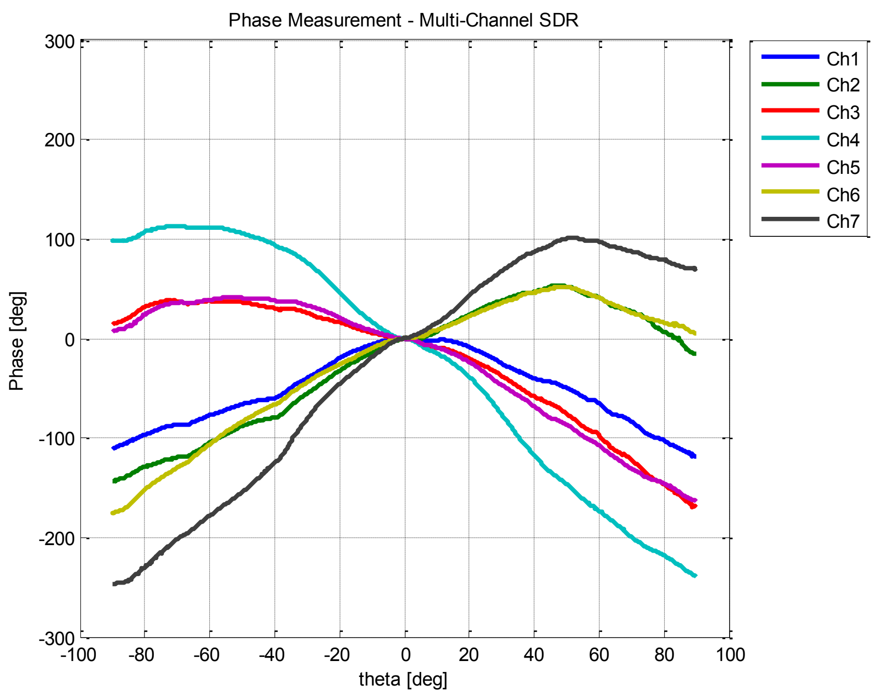

Figure 7-5. Phase multi-channel calibration method, all channels.

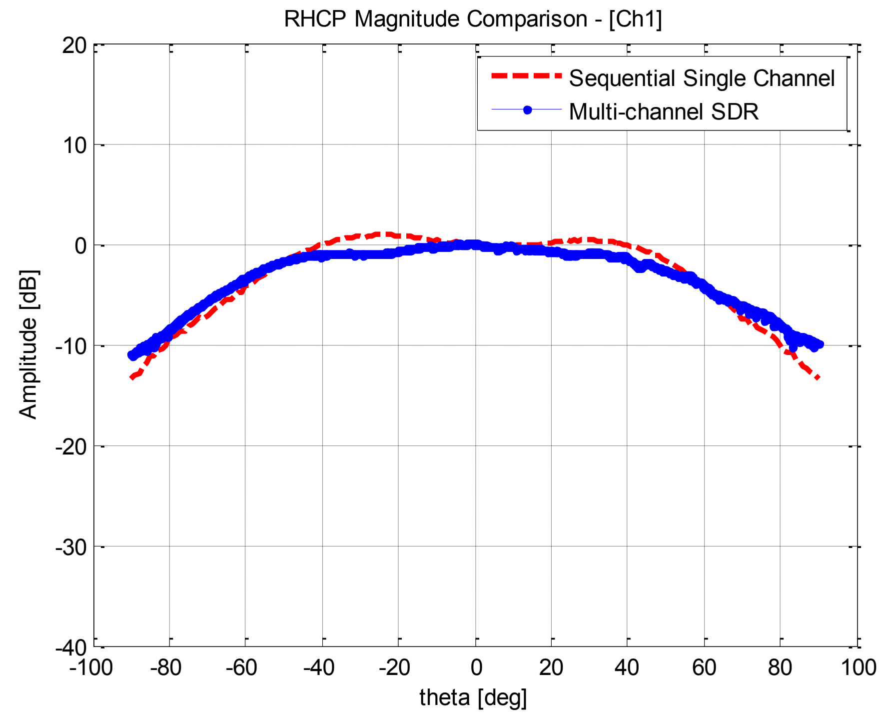

Figure 7-6. Magnitude comparison, element #1, reference element.

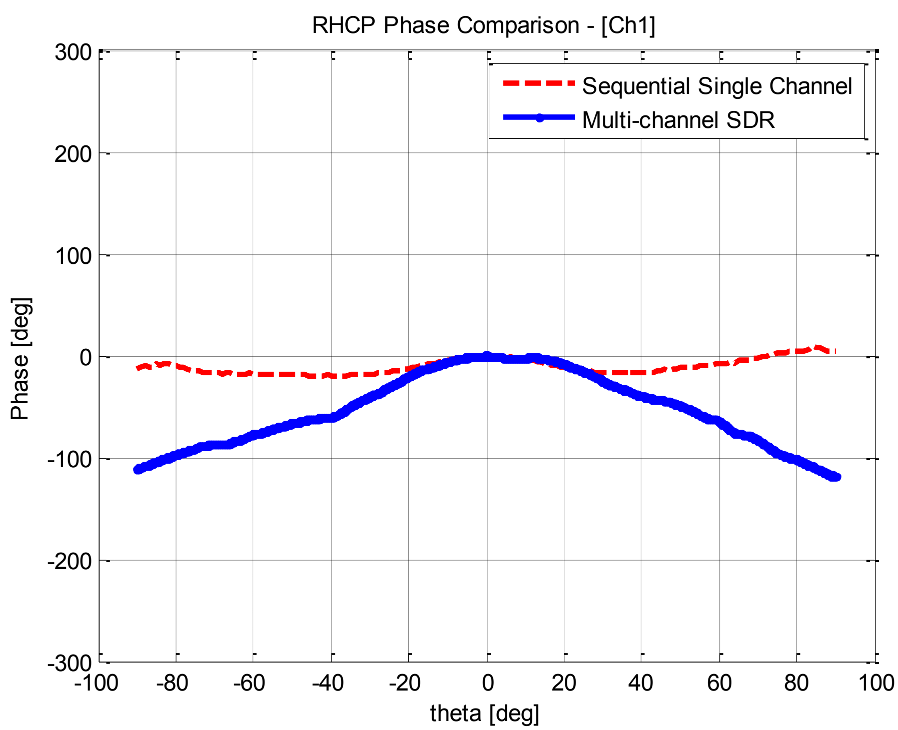

Figure 7-7. Phase comparison, element #1, reference element.

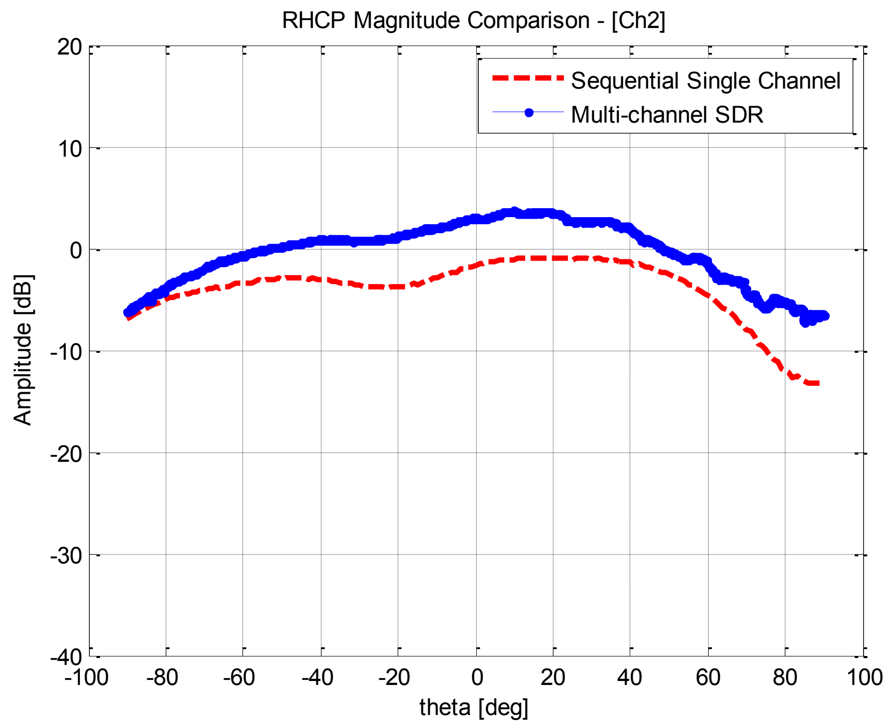

Figure 7-8. Magnitude comparison, element #2.

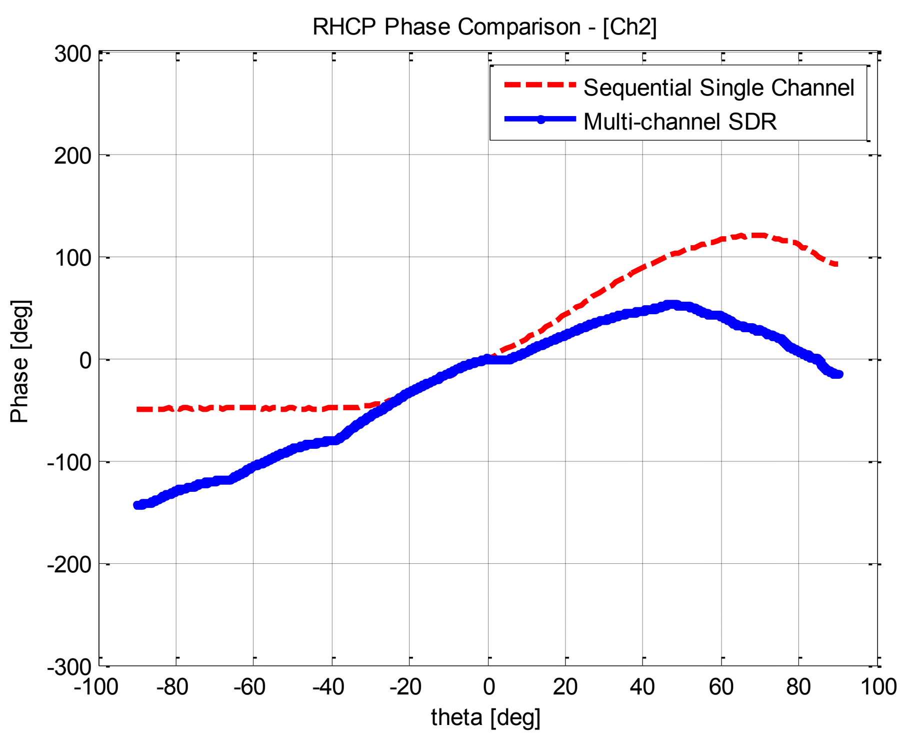

Figure 7-9. Phase comparison, element #2.

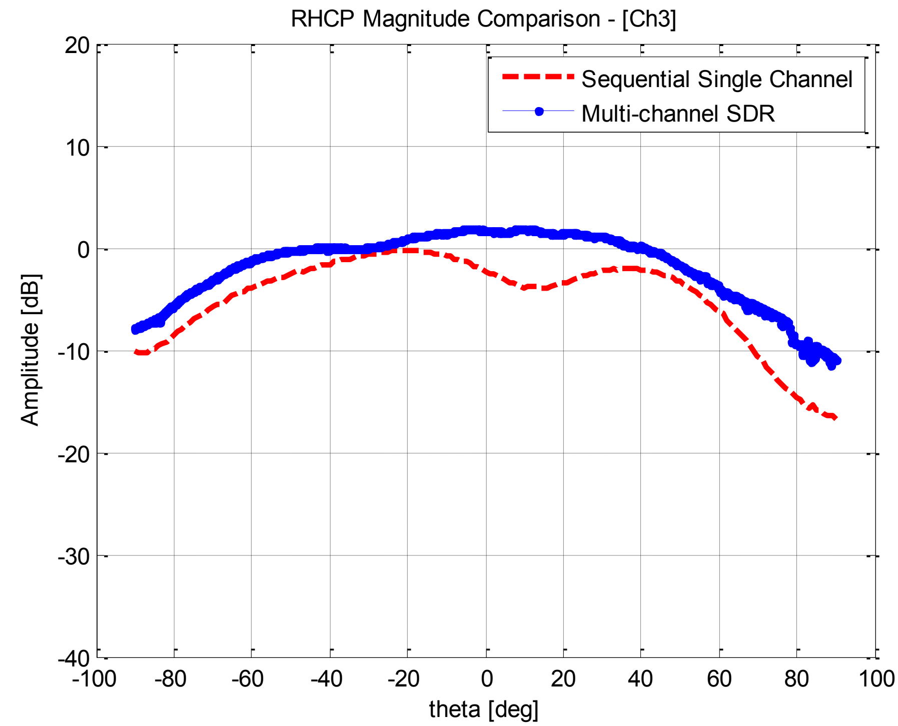

Figure 7-10. Magnitude comparison, element #3.

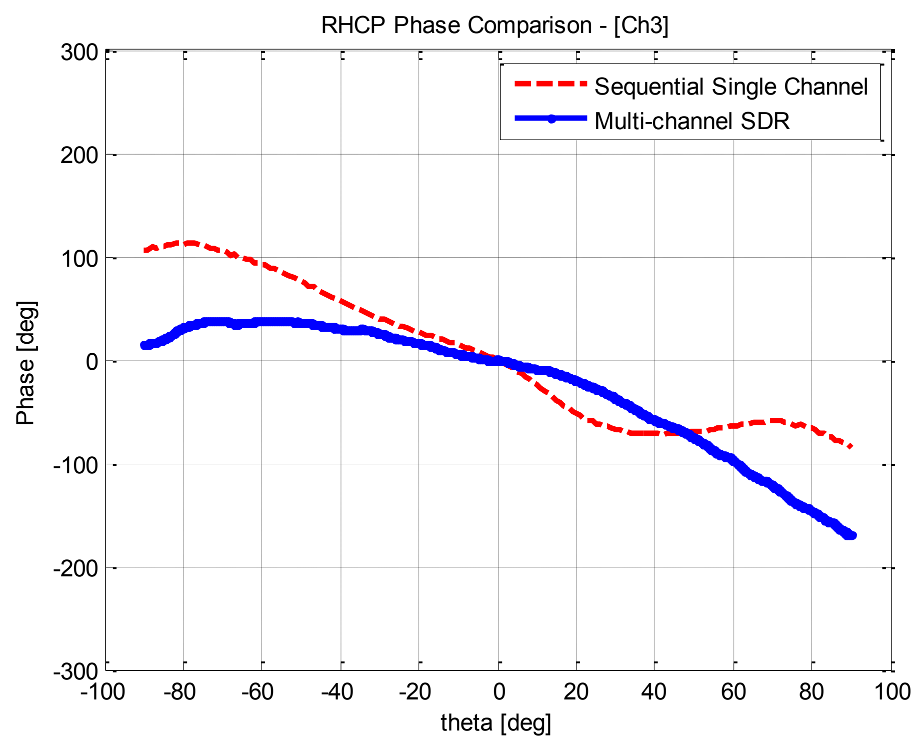

Figure 7-11. Phase comparison, element #3.

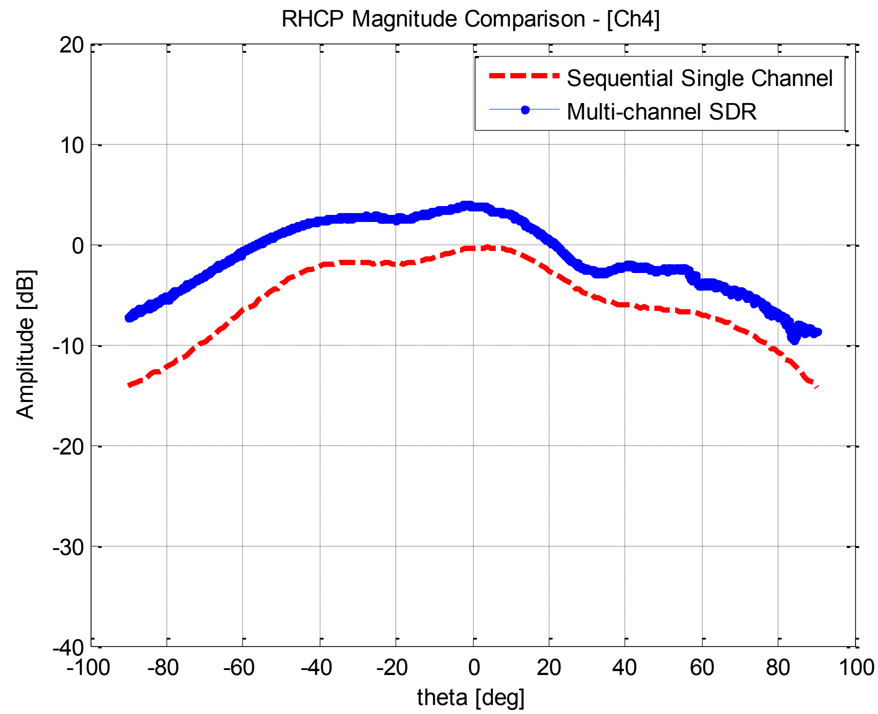

Figure 7-12. Magnitude comparison, element #4.

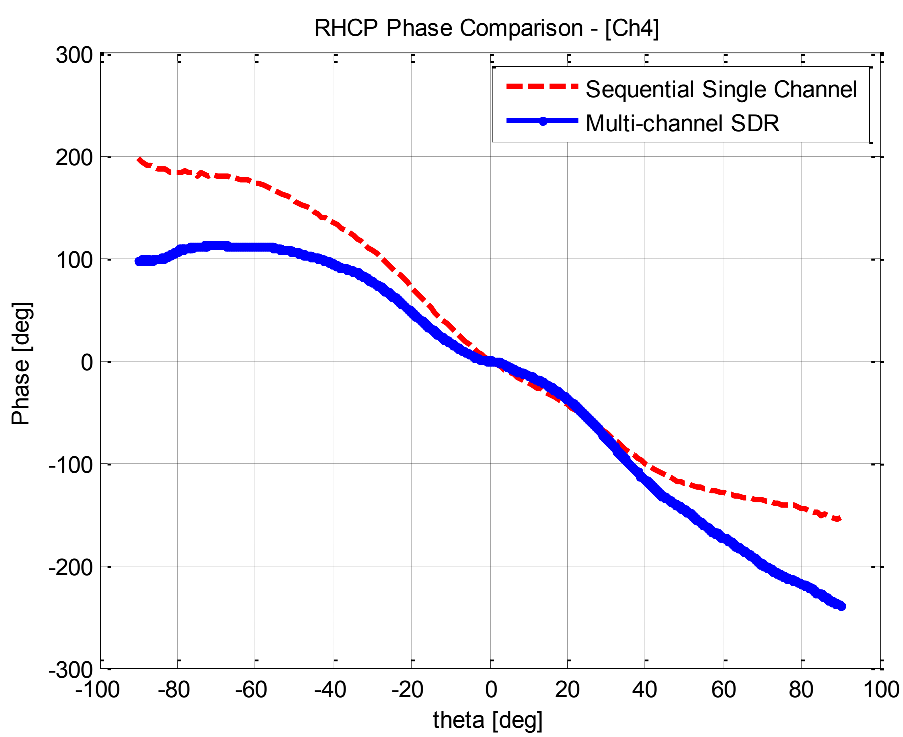

Figure 7-13. Phase comparison, element #4.

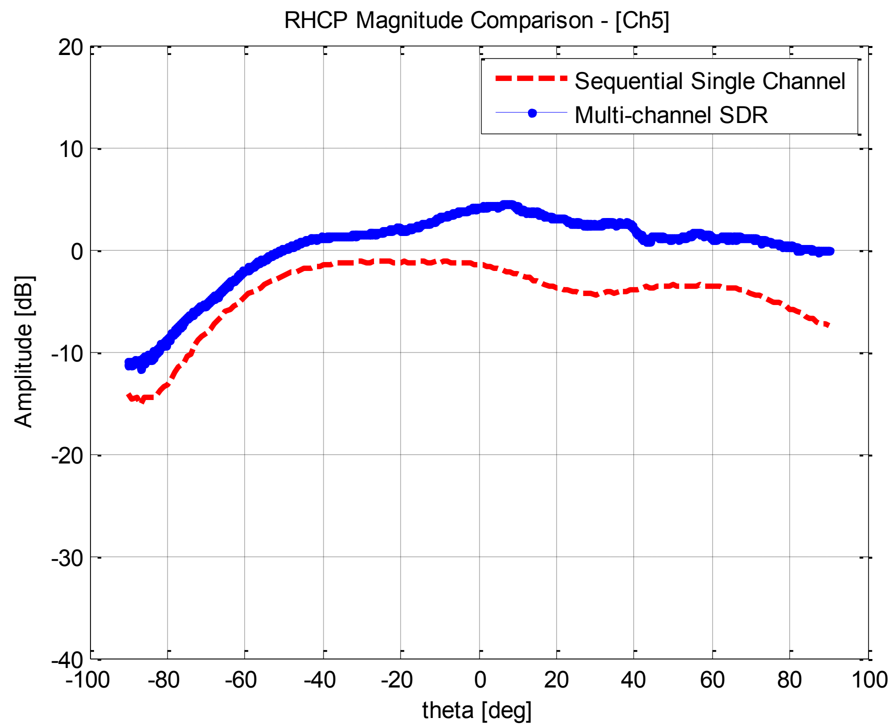

Figure 7-14. Magnitude comparison, element #5.

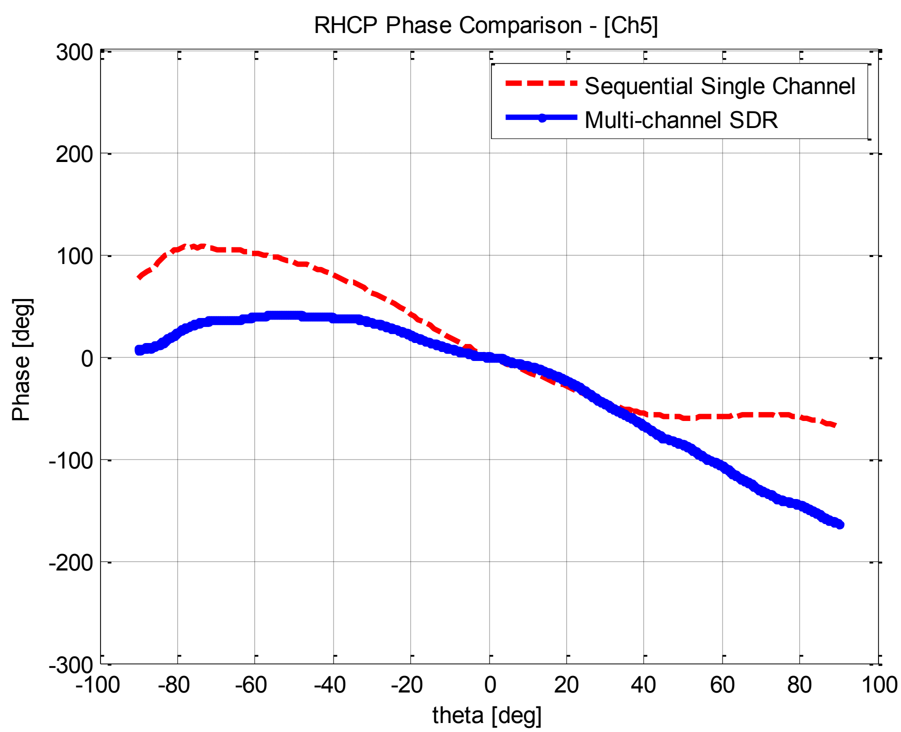

Figure 7-15. Phase comparison, element #5.

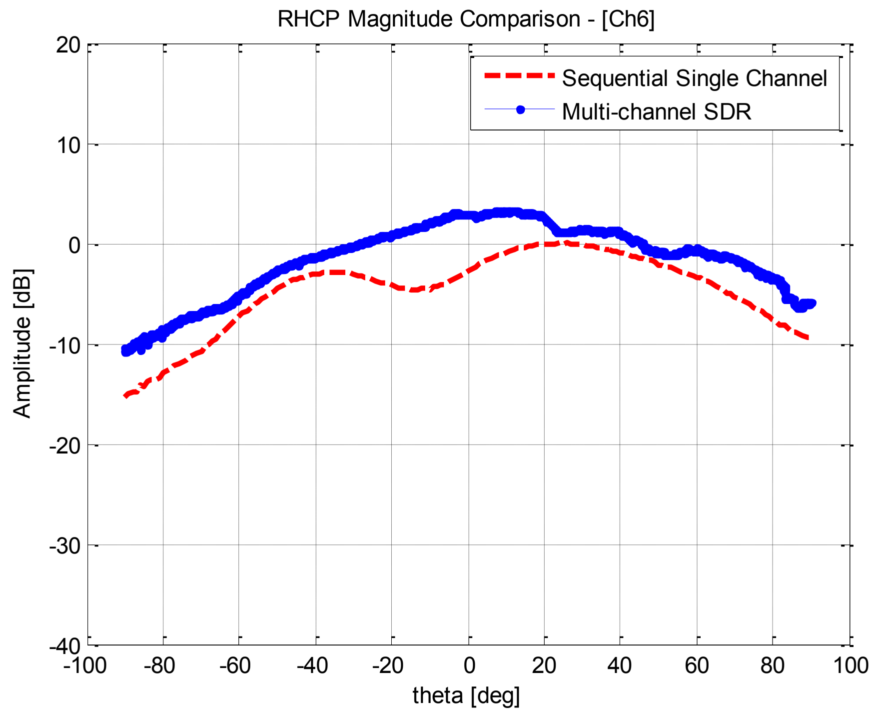

Figure 7-16. Magnitude comparison, element #6.

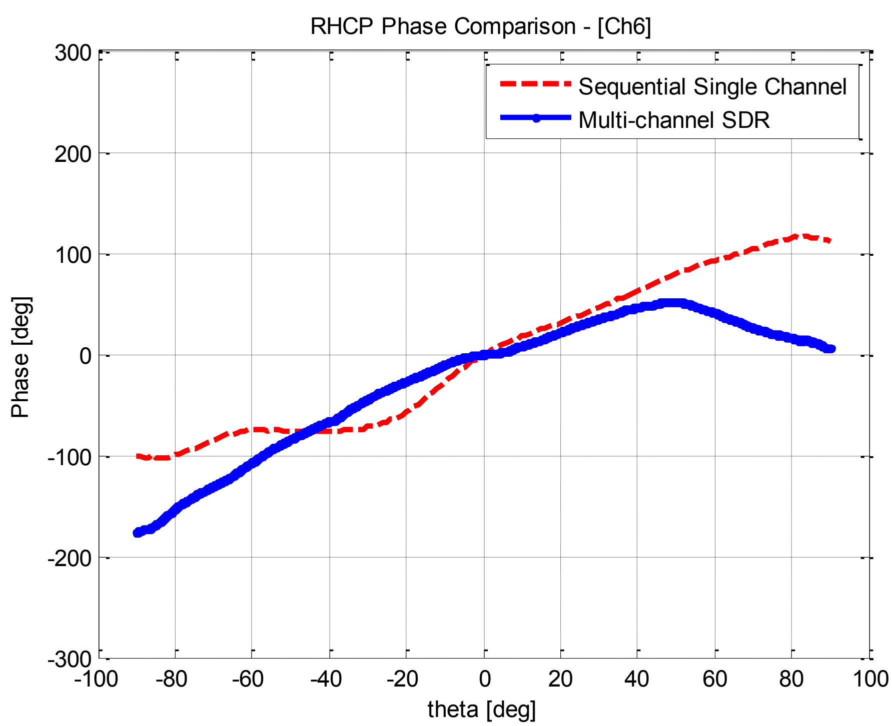

Figure 7-17. Phase comparison, element #6.

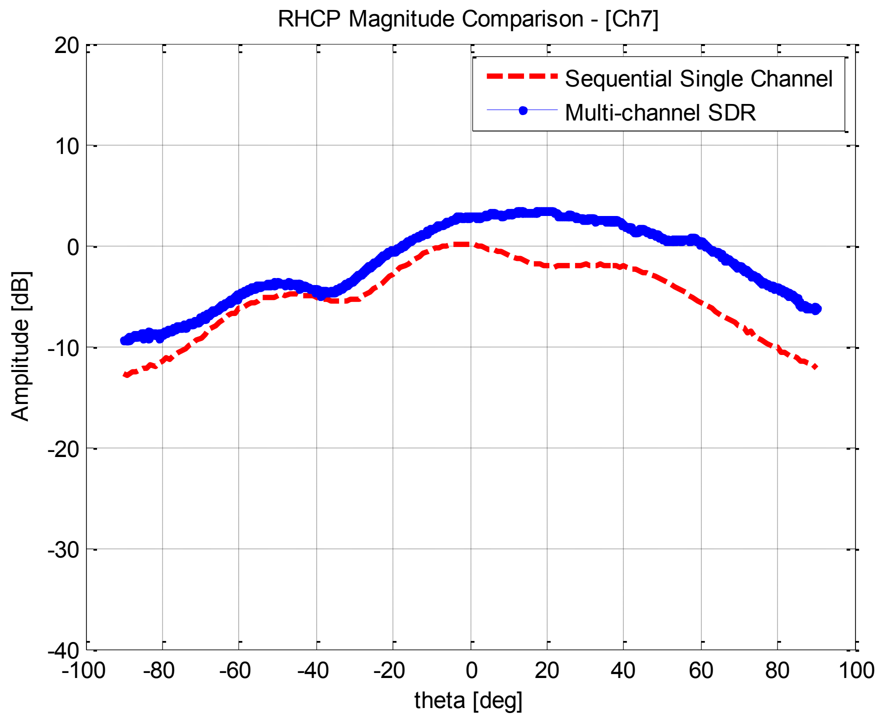

Figure 7-18. Magnitude comparison, element #7.

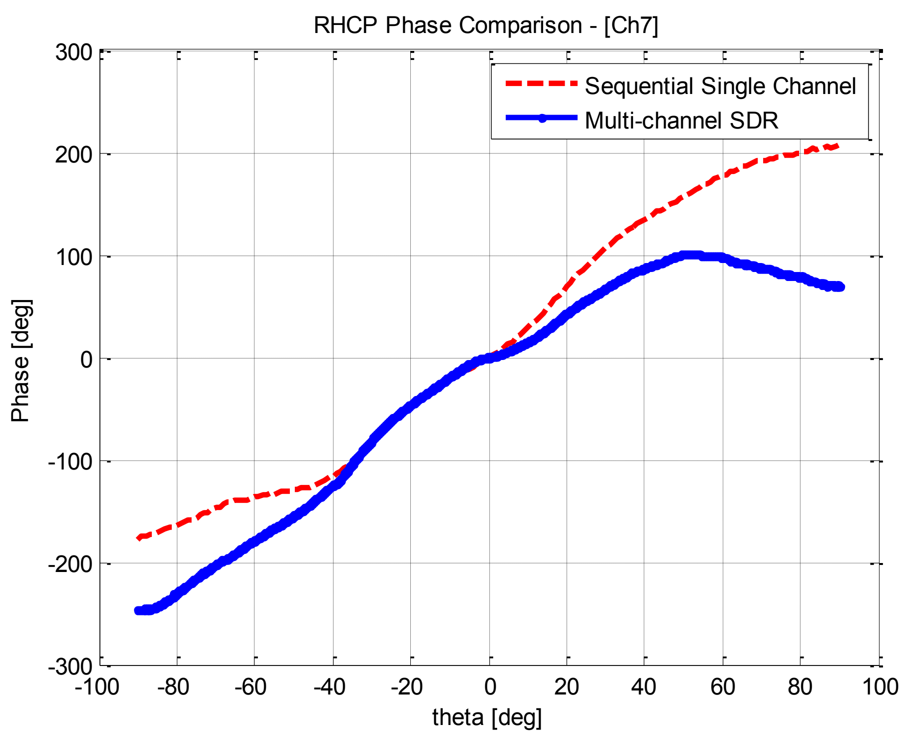

Figure 7-19. Phase comparison, element #7.

The calibration data results determined by the SDR multi-channel data acquisition system are compared with the calibration data results obtained with the traditional antenna test measurement methods. These comparisons show that the SDR multi-channel data acquisition calibration data results compare well with the traditional antenna single-element calibration data results. The magnitude and phase measurement results for each element of the CRPA are shown in Figure 7-2 through 7-5 for both the single-channel and multi-channel calibration methods, respectively. The single-channel and multi-channel calibration methods compare well to one another as represented in Figures 7-2 and 7-3, respectively. The magnitude of each element is dependent on its location on the array and the elevation angle. The single-channel method and multi-channel method have very similar amplitude characteristics.

The phase measurements for both the single-channel and multi-channel calibration methods are shown in Figures 7-4 and 7-5, respectively. The phase measurement results exhibit similar phase characteristics for each element as a function of elevation. Due to the orientation of the AUT, elements 2 and 6 exhibit similar phase variations and elements 3 and 5 exhibit similar phase variations; while elements 4 and 7 exhibit mirrored phase variations; this is because the phase variations for each element are dependent on their distance from the probe. At the beginning of the elevation measurement scan, the CRPA is at an elevation angle of -90º; here elements 2, 6, and 7 closer to the probe and elements 3, 4, and 5 are further from the probe. During the scan, the CRPA rotates around the z-axis and the elevation angle increases from -90º to 90º. As the elevation angle increases, the distance from the probe to elements 2, 6, and 7 increases, while the distance from the probe to elements 3, 4, and 5 decreases. The increase and decrease in elevation angle, for the respective elements, will result in variations in the phase measurement; this is because the elements are at different locations in the carrier wave cycle. At an elevation angle of 0º, the CRPA is at boresight and each element is relatively the same distance from the probe. To compensate for this effect, the lever arm could have been removed in post processing; however, since we are just comparing the calibration parameters for each calibration method this would not be productive. By not removing the lever arm it is easier to visually distinguish each element by the location and orientation in which it is mounted on the ground plane.

Additional variations in the phase measurement will arise when forming RHCP phase estimations as a result of the ground plane boundary conditions. At large incident angles (elevation angel near 0º) the co-pole wave component will have a much lower gain in comparison to the cross-pole wave component. Due to the boundary conditions of the ground plane, the tangential electric field vector inside the ground plane has to equal the electric field vector outside of the ground plane; as a result, the parallel (co-pole) wave component has less gain than the perpendicular (cross-pole) wave component at large incident angels [38]. When the wave components are combined to form RHCP measurements, the low gain of the co-pole component will decrease the overall magnitude and introduce phase variations.

Figures 7-6 through 7-19 show element by element phase and magnitude comparisons for both the single-channel and multi-channel calibration methods tested. The comparisons results show that the demonstrated multi-channel calibration method using a CRPA/SDR configuration produces similar antenna element characterization and magnitude and phase calibration measurements to the sequential single-channel calibration method. However, magnitude and phase measurements differences are present between the multi-channel and single-channel methods.

The measurement difference are a result of changes in power levels in the receiver system, the AGC, and higher-resolution of the multi-channel SDR system measurements, and because of still undetected measurement outliers. Additional measurement biases may have been introduced due to the manual elevation control implemented during testing. To correct for the measurement differences, the testing procedure can be improved upon to incorporate a more careful control of the testing setup, power levels, and system noise. One possible method of improving the testing setup would be to power up the pre-amps within each antenna element during single-channel sequential testing. This could be achieved by adding cables with bias tees in addition to the 50 Ω loads. With this method each element's pre-amp would be powered during both the single-channel sequential traditional method and the multi-channel testing method, possibly improving the measurements.

CHAPTER 8 CONCLUSION

This thesis presents a demonstrated method for the performance of a calibration method for a CRPA using a SDR configuration. The combination CRPA and SDR system consists of a low-cost 7-element configuration where the antenna RF inputs are fed directly into the multi-channel SDR system. This combination CRPA and SDR system was characterized in an anechoic chamber environment to closely replicate the fielded antenna/receiver system. This combined CRPA and SDR system configuration will provide multi-antenna element characterization and calibration measurements that can be used to remove carrier and/or code phase biases caused by the antenna elements and receiver front-end components for down-stream adaptive signal processing algorithms.

The objective of the thesis is to present the demonstrated method for the performance characterization of a calibration method for a CRPA and SDR configuration that closely represents the eventual fielded systems. This provides a method of calibration for an array using a real world CRPA/SDR system. For verification, the calibration data produced by the CRPA/SDR system configuration was compared with calibration data produced using a traditional sequential single-channel CRPA test approach where each element of the array is characterized one at a time with a traditional antenna test approach.

The traditional calibration test method was first performed using the CRPA to determine “truth measurements” for the magnitude and phase of each element in the CRPA. Each antenna element was tested separately by connecting one individual element to the vector network analyzer and placing 50Ω impedance loads on the remaining elements. The vector network analyzer determined the magnitude and phase measurements of each element over various azimuth and/or elevation angles. During testing, each AUT element was rotated 180º in elevation and 360º in the azimuth for both co- and cross-polarization. The co- and cross-polarization data was then combined to form RHCP calibration measurements.

The second method using the same 7-element CRPA and the SDR multi-channel data acquisition system was then tested in the anechoic chamber. Each antenna element was connected to the SDR RF front-ends using LMR-195 cable assemblies. For these demonstration tests, a CW signal was generated by a Agilent RF signal generator, that was phase locked to the SDR receiver system. This setup allowed for simultaneous data collection for each of the seven antenna elements of the CRPA. Multiple tests were performed by rotating the AUT across the azimuth and/or elevation plane. The digital data was stored, and the magnitude and phase measurements where determined in post-processing.

The calibration data results determined by the SDR multi-channel data acquisition system were then compared with the calibration data results obtained with the traditional antenna test measurement methods. These comparisons show that the SDR multi-channel data acquisition calibration data results compare very well with the traditional antenna single-element calibration data results; however, the SDR multi-channel data acquisition system provides several advantages. These advantages include higher resolution amplitude and phase response measurements and a more representative CRPA/SDR configuration that would be fielded. Thus, not only are the RF characteristics of the CRPA antenna characterized, but also the RF front-end of the SDR RF front-end all the way up to the point where the signals are digitized. This thesis also highlights that the calibration corrections as well as the antenna steering algorithm can be implemented in one step with in the SDR.

The work in this thesis is significant because it provides a calibration method that implements the actual CRPA/SDR system that would be used in real world applications. Using a CRPA/SDR configuration is advantageous because it provides added flexibility for antenna electronics that are used to perform adaptive processing techniques and error mitigation, whereby these functions could be implemented within the SDR. With the CRPA/SDR system, the antenna calibration and adaptive processing can be done with embedded signal processing software. This allows the receiver system to be application specific and easily upgradable. It also allows for multiple processing techniques to be implemented on the same set of data within the embedded software of the receiver system.

8.1 Future Work

Additional research can be implemented to continue the test procedures and data analysis of the demonstrated multi-channel calibration method for a CRPA/SDR receiver system. This includes additional calibration and measurement testing in the anechoic chamber to improve the signal quality of the magnitude and phase measurements and remove measurement outliers present in the system. One method of improving the testing setup would be to power up the pre-amps within each antenna element during both single-channel and multi-channel testing. Additionally, the measurement biases induced by adaptive signal processing algorithms and the effects they produce when implementing the demonstrated multi-channel calibration method with a CRPA/SDR configuration can be further investigated. This can be done by measuring the amplitude and phase variations of the CRPA/SDR system when implementing STAP beam forming and/or null steering algorithms embedded in the SDR in the presence of multiple interference sources and jammers. Additionally, the testing system can add a GNSS signal as the source to characterize group delay.

BIBLIOGRAPHY

[1] Pratap Misra and Per Enge, *Global Positioning System Signals, Measurements, and Performance*, 2nd ed. Lincoln, Massachusetts, United States: Ganga-Jamuna Press, 2006.

[2] Sanjeev Gunawardena, "Feasibility Study for the Implementation of Global Positioning System Block Processing Techniques in Filed Programmable Gate Arrays," Ohio University, Athens, OH, Thesis 2000. [Online]. http://www.ohio.edu/people/starzykj/network/research/thesis/sanjeev-thesis.pdf

[3] Ian Matthew Barton, "Antenna Performance Analysis for the Nationwide Differential Global Positioning System," Ohio University, Athens, Thesis 2005. [Online]. http://etd.ohiolink.edu/view.cgi?acc_num=ohiou1126820930

[4] David S. De Lorenzo, "Navigation Accuracy and Interference Rejection for GPS Adaptive Antenna Arrays," Standford University, Stanford, CA, Dissertation 2007.

[5] Ung Suok Kim, David De Lorenzo, Jennifer Gautier, Per Enge, and John A. Orr, "Phase Effects Analysis of Patch Antenna CRPAs for JPALS," in *ION GNSS 17th International Technical Meeting of the Satellite Division*, Long Beach, CA, 2004, pp. 1531-1538.

[6] Ung Suok Kim, "Mitigation of Signal Biases Introduced by Controlled Reception Pattern Antennas in a High Inegrity Carrier Phase Differential GPS System," Stanford University, Stanford, CA, Disstertation 2007.

[7] Gary A. McGraw, S.Y. Young Young, and Kristen Reichenauer, "Evaluation of GPS Anti-Jam System Effects on Pseudorange and Carrier Phase Measurements for Precision Approach and Landing," in *ION GNSS 17th International Technical Meeting of the Satellite Division*, Long Beach, CA, 2004, pp. 2742-2751.

[8] Sai K Kalyanaraman, "High Accuracy GPS Phase Tracking Under Signal Distortion," Ohio University, Athens, OH, Dissertation 2009.

[9] Michael Braasch, "Spread-Spectrum Ranging Multipath Model Validation," *IEEE Transactions on Aerospace and Electronic Systems*, 2001, vol. 37, no. 1, pp. 298-304.

[10] Christopher M. Church and Inder J. Gupta, "Calibration of GNSS Adaptive Antennas," in *22nd International Meeting of the Satellite Division of the Institute of Navigation*, Savannah, GA, 2009, pp. 344-350.

[11] James R. Huddle and R. Grover Brown, "Multisensor Navigation Systems," in *Avionics Navigation Systems*, 2nd ed., Myron Kayton and Walter R. Fried, Eds. New York, United States of America: John Wiley & Sons, Inc., 1997, ch. 3, pp. 55 - 96.

[12] Min Li, Feixue Wang, Asghar Tabatabaei Balaei, Andrew Dempster, and Chris Rizos, "A GNSS Software Receiver Beamforming Architecture," in *International Symposium on GPS/GNSS*, Tokyo, Japan, 2008, pp. 904-909.

[13] Jonathan A. Ulrey and Inder J. Gupta, "Optimum Element Distribution for Circular Adaptive Antenna Systems," in *ION NTM*, Monterey, CA, 2006, pp. 76-81.

[14] Andrew J. O'Brien and Inder J. Gupta, "Otimum Adaptive Filtering for GNSS Antenna Arrays," in *ION GNSS 21st International Technical Meeting of the Satellite Division*, Savannah, GA, 2008, pp. 2796-2805.

[15] Christopher Church, Inder Gupta, and Andrew O'Brien, "Adaptive Antenna Induced Biases in GNSS Receivers," in *ION 63rd Annual Meeting*, Cambridge, Massachusetts, 2007, pp. 204-212.

[16] National Geodetic Survey. (2012, March) National Geodetic Survey - Antenna Calibration FAQ. [Online]. http://www.ngs.noaa.gov/ANTCAL/FAQ.jsp

[17] Andria Bilich, Charles Geoghegan, Gerald Mader, Giovanni Sella, and Dennis Lokken. (2011, August) National Geodetic Survey GNSS Antenna Calibration Policy. [Online]. http://www.ngs.noaa.gov/ANTCAL/Antcal_policy.pdf

[18] National Geodetic Survey. (2012, March) National Geodetic Survey - Antenna Calibrations. [Online]. http://www.ngs.noaa.gov/ANTCAL/

[19] Andria Bilich and Gerald L. Mader, "GNSS Absolute Antenna Calibration at the National Geodetic Survey," in *23rd International Technical Meeting of the Satellite Division of The Institute of Navigation*, Portland, OR, 2010, pp. 1369-1377.

[20] Geo++ GmbH. (2012, November) Geo++. [Online]. http://www.geopp.de/media/docs/AOA_DM_T/general.html

[21] Merril I. Skolnik, *Introduction to Radar Systems*, 3rd ed.: McGraw - Hill, 2002.

[22] Chris Bartone and Tom Stansell, "A Multi-Circular Ring CRPA for Robust GNSS Performance in an Interference and Multipath Environment," in *ION NTM*, 2011.

[23] Toby Haynes. (1998, March 26) A Primer on Digital Beamforming. Technical Document. [Online]. www.spectrumsignal.com/publications/beamform_primer.pdf

[24] Constantine A. Balanis, "Smart Antennas," in *Antenna Theory: Analysis and Design*, 3rd ed., Constantine A. Balanis, Ed. Hoboken, NJ, United States of America: John Wiley & Sons, Inc., 2005, ch. 16, pp. 945 - 994.

[25] Alison Brown and David Morley, "Test Results of a 7-Element Small Controlled Reception Pattern Antenna," in *ION GPS,2001*, Salt Lake City, Utah, 2001, pp. 1-8.

[26] Gary A. McGraw, Ryan S.Y. Young, Kristen Reichenauer, Jeff Stevens, and Fred Ventrone, "GPS Multipath Mitigation Assessment of Digital Beam Forming Antenna Technology in a JPALS Dual Frequency Amoothing Architecture," in *ION NTM 2004*, San Diege, CA, 2004, pp. 562-572.

[27] Sanjeev Gunwardena, "GNSS Receiver Design 2: Baseband Signal Processing & Implementation," in *ION GNSS 2011 Tutorial*, Portland, OR, 2011, pp. 9-70.

[28] Elliot D. Kaplan, *Understanding GPS: Principles and Applications*, 2nd ed., Christopher J. Hegarty, Ed. Norwood, MA, USA: ARTECH HOUSE, INC., 2006.

[29] Rodney G. Vaughan, Neil L. Scott, and D. Rod White, "The Theory of Bandpass Sampling," *IEEE Transactions of Signal Processing*, 1991, vol. 39, no. 9, pp. 1973-1984.

[30] Frank van Graas, Chris Bartone, and Tom Arthur, "GPS Antenna Phase and Group Delay Corrections," in *ION NTM*, San Diego, CA, 2004, pp. 399-408.

[31] Gerald L. Mader and Neil D. Weston, "GPS Antenna Calibration at the National Geodetic Survey, NOS/NOAA," in *FIG Working Week*, Stockholm, Sweden, 2008. [Online]. ftp://ftp.ngs.noaa.gov/pub/corbin/geomatics-vendor-summit/day02/10-mader_antenna-calibration.ppt

[32] Gary A. McGraw, Charles McDowell, Ryan S.Y. Young, and David W. Glessner, "Assessment of GPA Anit-Jaming System Pseudorange and Carrier Phase Measurement Error Effects," in *ION GNSS 18th International Technical Meeting of the Satellite Division*, Long Beach, CA, 2005, pp. 603-617.

[33] Andrew J. O.Brian, "Adaptive Antenna Arrays for Precision GNSS Receivers," The Ohio State University, Columbus, Dissertation 2009. [Online]. http://etd.ohiolink.edu/view.cgi?acc_num=osu1259170076

[34] Sanjeev Gunawardena and Frank Van Graas, "Multi-Channel Wideband GPS Anomalous Event Monitor," in *24th International Technical Meeting of the Sattellite Division of The Institute of Navigation*, Portland, OR, 2011, pp. 1957-1968.

[35] A.J. Van Dierendonck, "GPS Receivers," in *Global Positioning System: Theory and Applications Volume I*, Penina Axelrad and Per Enge, Eds. Los Altos, CA, United States of America: American Institute of Aeronautics and Astronautics, Inc., 1996, ch. 8, pp. 329-405.

[36] Antcom CORP., Center Connector 2in Square Active L1/L2 GPS Antenna, April 1, 2010, P/N: 1G1215A-XXC-X, Rev: A, CC: 3CVE1.

[37] Ohio University Avionics Engineering Center. (2012, August) Ohio University Avionics Engineering Center Website. [Online]. http://www.ohio.edu/avionics/facilities/anechoic-chamber.cfm

[38] Matthew N.O. Sadiku, *Elements of Electromagnetics*, 5th ed. New York, USA: Oxford University Press, 2009.

[39] "GPS Antenna Calibration at the National Geodetic Survey,". [Online]. ftp://ftp.ngs.noaa.gov/pub/corbin/geomatics-vendor-summit/day02/10-mader_antenna-calibration.ppt

APPENDIX: CYCLE SLIP PHASE ERROR

The following error graphs illustrate the number of phase cycle slips that occurred due to outlier measurements during software baseband processing. The results were calculated by determining the number of cycle slips that occurred within each 20ms PDI accumulation time for both the co-polarization and cross-polarization phase estimates. The error graphs show that the majority of the cycle slips occurred at larger incident angles when measuring the co-polarization phase estimate.

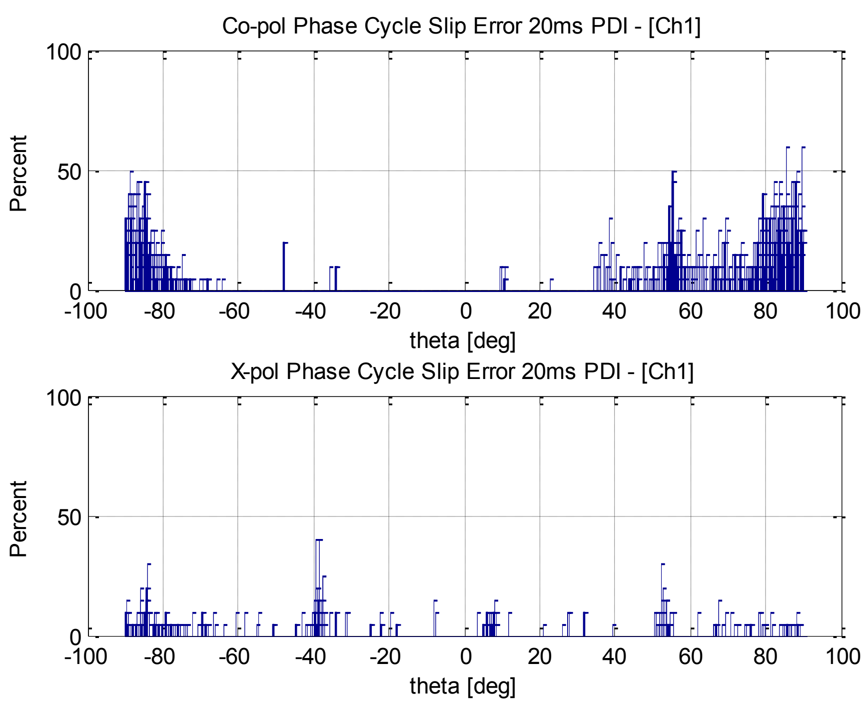

Figure A1-1. Cycle Slip Phase Error, element #1

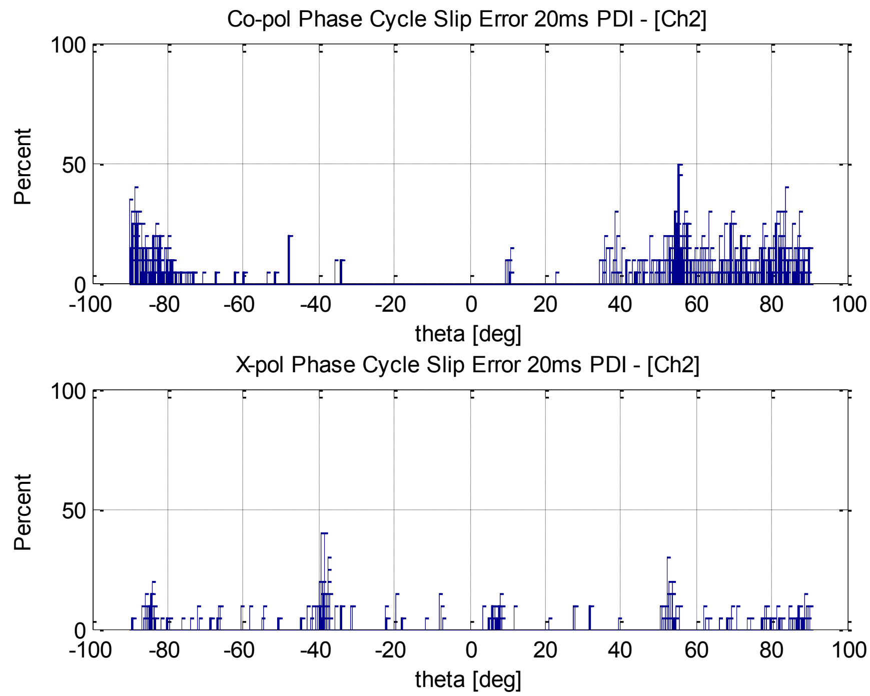

Figure A1-2. Cycle Slip Phase Error, element #2

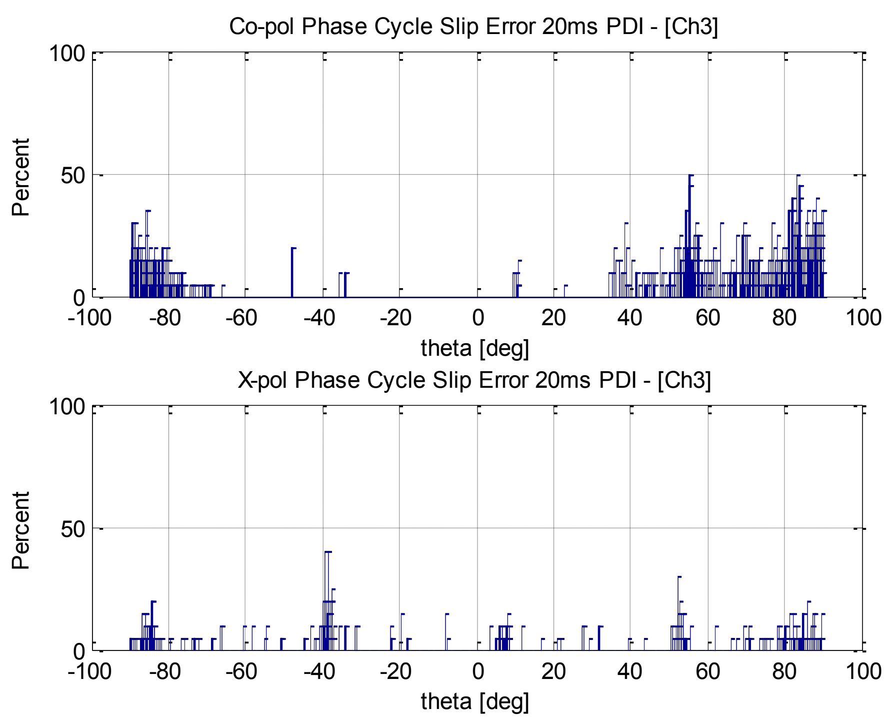

Figure A1-3.Cycle Slip Phase Error, element #3

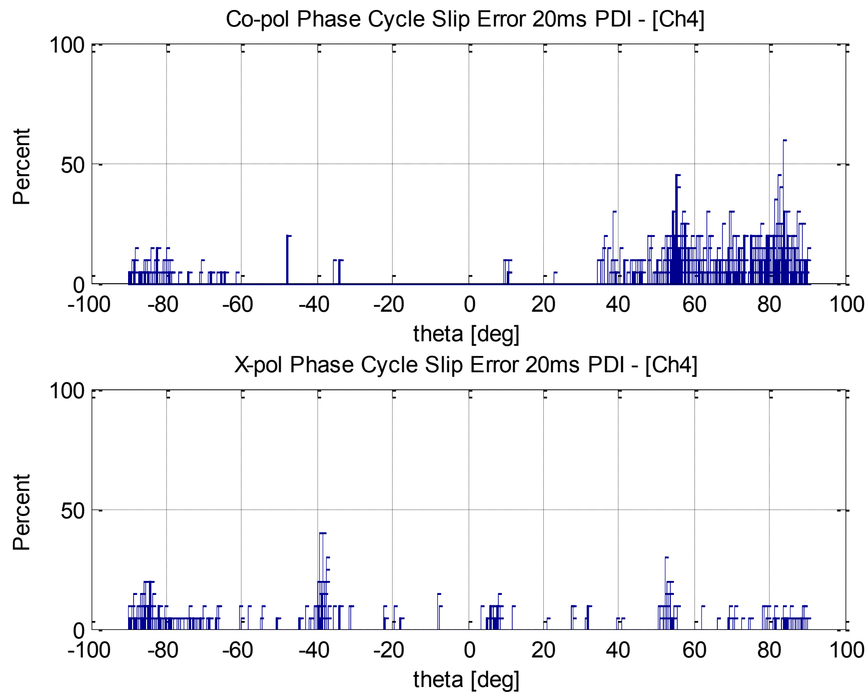

Figure A1-4. Cycle Slip Phase Error, element #4

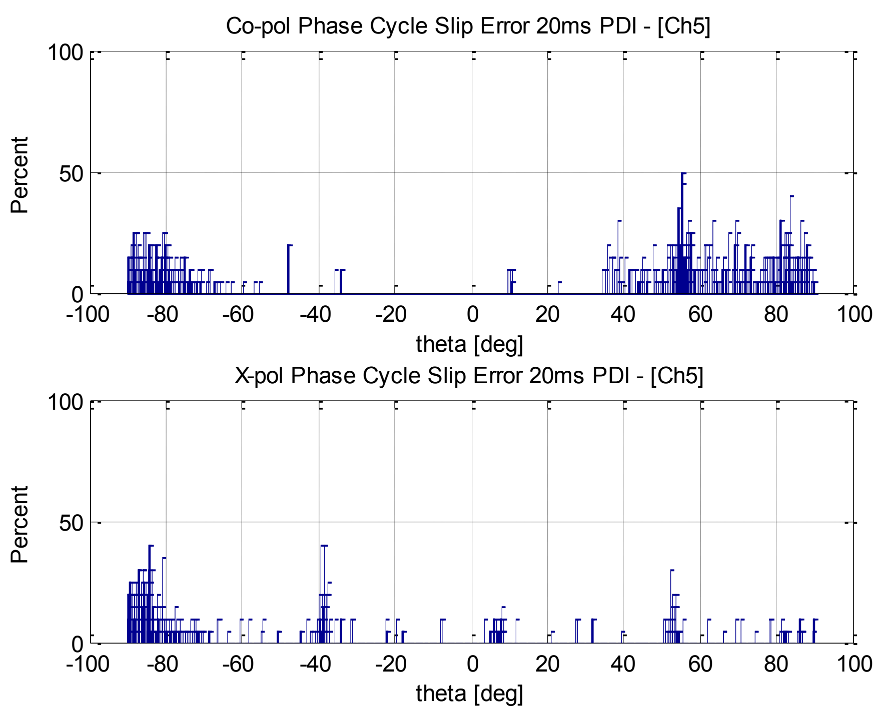

Figure A1-5. Cycle Slip Phase Error, element #5

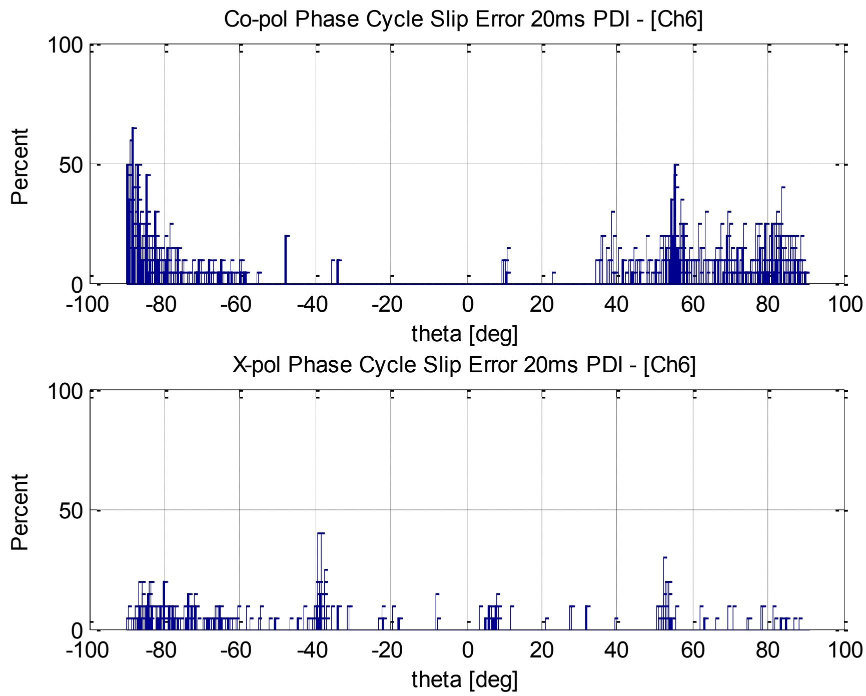

Figure A1-6. Cycle Slip Phase Error, element #6

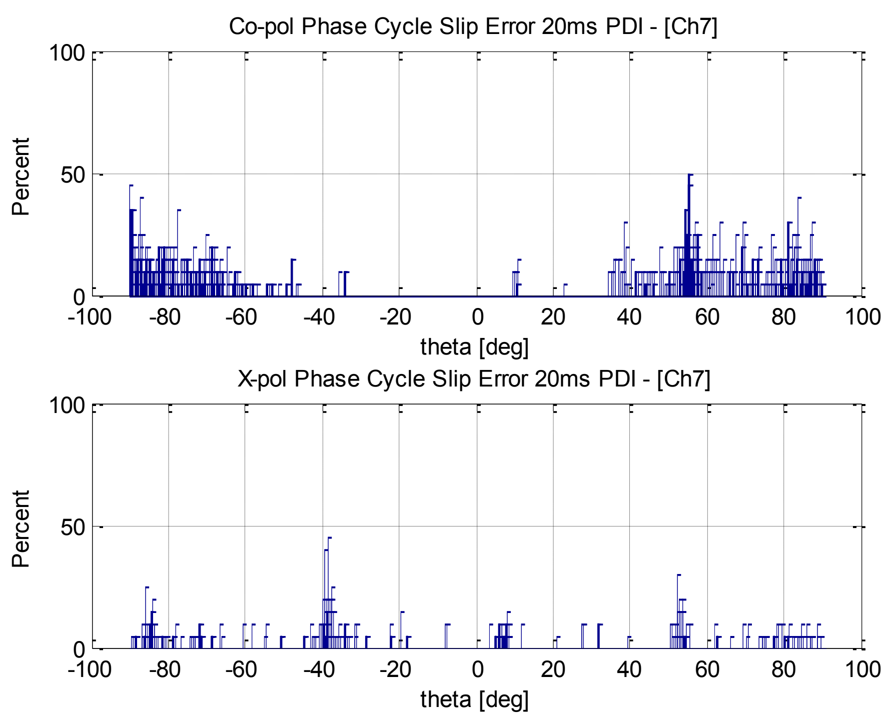

Figure A1-7. Cycle Slip Phase Error, element #7